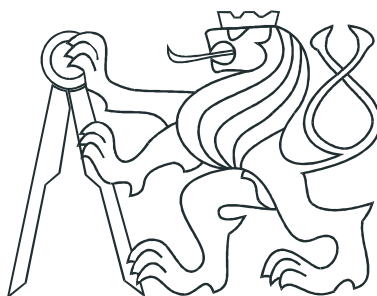


CZECH TECHNICAL UNIVERSITY IN
PRAGUE

Faculty of Nuclear Sciences and Physical
Engineering

Department of Physics



Bachelor thesis

Correlation femtoscopy study of
nucleus-nucleus collisions dynamics at the
STAR experiment

Jindřich Lidrych

Supervisor: RNDr. Petr Chaloupka, Ph.D.

Prague, 2014

ČESKÉ VYSOKÉ UČENÍ TECHNICKÉ
V PRAZE

Fakulta jaderná a fyzikálně inženýrská

Katedra fyziky



Bakalářská práce

Studium dynamiky jádro-jaderných
srážek pomocí korelační femtoskopie
na experimentu STAR

Jindřich Lidrych

Vedoucí práce: RNDr. Petr Chaloupka, Ph.D.

Praha, 2014

Prohlášení:

Prohlašuji, že jsem svou bakalářskou práci vypracoval samostatně a použil jsem pouze podklady (literaturu, software, atd.) uvedené v příloženém seznamu.

Nemám závažný důvod proti užití tohoto školního díla ve smyslu 60 Zákona .121/2000 Sb., o právu autorském, o právech souvisejících s právem autorským a o změně některých zákonů (autorský zákon).

V Praze dne 21.července 2014

Jindřich Lidrych

Title:

Correlation femtoscopy study of nucleus-nucleus collisions dynamics at the STAR experiment

Author: Jindřich Lidrych

Specialization: Experimental nuclear physics

Sort of project: Bachelor thesis

Supervisor: RNDr. Petr Chaloupka, Ph.D.

Abstract: High energy heavy ion collisions provide means to study properties of nuclear matter under the extreme conditions. It is expected that a new state of matter called quark-gluon plasma is created during these collisions. However this system exists only for a brief period of time with typical space and time extents on the order of 10^{-14}m .

This thesis discusses two-particle correlation femtoscopy which is the most widely used experimental tool for measuring characteristic sizes and life-times of the created system. This work reviews the basic theoretical foundations of the femtoscopic measurements and presents overview of the most important STAR results in this field.

Key words: Correlation femtoscopy, quark-gluon plasma, heavy ion collision, STAR detector, blast wave model.

Název práce:

Studium dynamiky jádro-jaderných srážek pomocí korelační femtoskopie na experimentu STAR

Autor: Jindřich Lidrych

Abstrakt: Vysokoenergetické srážky těžkých iontů jsou klíčem ke studiu jaderné hmoty za extrémních podmínek. Očekává se, že během nich může dojít k vytvoření nové fáze jaderné hmoty, tak zvaného kvark-gluonové plazmatu. Tento stav hmoty však existuje pouze velmi krátce. Typické časo-prostorové rozměry tohoto systému jsou řádu 10^{-14} m.

Jedna z možností jak studovat tento systém je pomocí dvoučásticové korelační femtoskopie, která je představena v této bakalářské práci. V práci jsou rozebrány teoretické základy femtoskopických měření spolu s přehledem a diskusí nejvýznamnějších femtoskopických měření, které provedl experiment STAR.

Klíčová slova: Korelační femtoskopie, kvark-gluonové plazma, srážky těžkých iontů, STAR detektor, blast wave model.

Acknowledgement

I would like to thank all people, who supported me during the working on this bachelor thesis. Especially to RNDr. Petr Chaloupka, Ph.D. for his patience, professional and valuable advice, friendly attitude and language corrections.

Contents

1	Physics of heavy ion collisions	12
1.1	Quarks and Leptons	12
1.2	Fundamental interaction	14
1.2.1	Strong interaction and Asymptotic freedom	15
1.3	Quark-gluon plasma	15
1.3.1	Signatures for Quark-gluon plasma	18
1.4	Nucleus-Nucleus Collisions	19
1.4.1	Kinematic Variables	20
1.4.2	Collision evolution	21
2	STAR experiment at RHIC	23
2.1	Relativistic Heavy Ion Collider	23
2.2	STAR detector	26
2.2.1	Time Projection Chamber	26
2.2.2	Time Of Flight detector	29
2.2.3	Barrel Electromagnetic Calorimeter	31
2.3	STAR trigger system	32
2.4	On-going upgrade of the STAR detectors	33
2.4.1	Muon Telescope Detector	33
2.4.2	Heavy Flavor Tracker	33
2.5	Future of the STAR detector	34
3	Correlation femtoscopy	35
3.1	Historical background of femtoscopy	35
3.2	Correlation function	35
3.3	Coordinate Systems	40
3.4	Parametrization of correlation function	41
3.5	Femtoscopic measurements	44
3.5.1	Signal Construction	45
3.5.2	Background Construction	45
3.5.3	Corrections	46
3.5.4	Fitting	47

4	Effect of dynamics on measured HBT observables	50
4.1	First order phase transition and "HBT puzzle"	50
4.2	Blast wave model/parametrization	52
4.3	Collective behaviour - m_T scaling / m_T dependence	55
4.3.1	Longitudinal flow	55
4.3.2	Transverse flow	56
5	Non-identical particle correlations	58
5.1	Non-identical particle and correlation function	58
5.2	Results from rare and non-identical particle correlations measure- ments	61
5.2.1	$\pi - \Xi$ correlations	62
5.2.2	$K^0 - K^0$ correlations	64
5.2.3	$p - \Lambda$ correlations	66
6	Conclusions	68
	Appendices	70
A	The RHIC Run Overview	71

List of Figures

1.1	Standard model	13
1.2	Coupling constant	16
1.3	Temperature dependence of the strong potential	16
1.4	QCD matter phase diagram	17
1.5	Collision of two nuclei	20
1.6	Heavy ion collision	21
2.1	Relativistic Heavy Ion Collider	24
2.2	PHENIX detectors	25
2.3	STAR detector	26
2.4	Time Projection Chamber	27
2.5	Anode pad	28
2.6	Trajectories of particles, which was reconstructed by using TPC .	29
2.7	Result from measuring dE/dx	30
2.8	Result from data analysis from the TOF	30
2.9	View of BEMC module	31
2.10	Heavy Flavor Tracker	33
2.11	eRHIC	34
3.1	Result of measurement of enhancement of $\pi^-\pi^-$ and $\pi^+\pi^+$ pairs.	36
3.2	Schema of emission particle.	37
3.3	Bertsch-Pratt coordinate system.	41
3.4	Source size dependence on the angle Φ , from which the source is observed.	43
3.5	Results of the measurement the HBT radii from the azimuthal sensitive analysis the pion distribution.	44
3.6	Application of corrections on measured correlation function. . . .	47
3.7	Comparison of the results from the fitting	49
4.1	Prediction of the first order phase transition	51
4.2	Results from two last decades.	51
4.3	Illustration of the blast wave model.	54
4.4	Homogeneity region	55
4.5	World data set m_T dependence of HBT parameters	56
4.6	Universality of m_T dependence for different particle mass	57

5.1	Illustration of the emission and interaction of two non-identical particle	59
5.2	Results of measured pion-kaon correlations.	60
5.3	Comparison of results (noted by \circ of measured shifted mean emission point with model prediction	61
5.4	Results from $\pi - \Xi$ correlations	63
5.5	Results from $K^0 - K^0$ correlations	65
5.6	Results from $p - \Lambda$ correlations	67

List of Tables

5.1	The overview of the femtosopic studies	62
A.1	The RHIC Run Overview	71
A.2	The RHIC Run Overview	72

Chapter 1

Physics of heavy ion collisions

For a long time people wanted to know the basic structure of matter. Already in ancient Greece some people believed that everything is made from a few basic elements. One of this people was Leucippus(490-420 BC)[1]. His atomic theory about these basic elements, which were called atoms, was developed by Democritus (460-370 BC)[1]. Their idea was basically correct, but unfortunately due to Aristotle(384-322 BC)[1], who was one of the greatest ancient philosopher, and his large influence the atomic theory was ignored. His idea about the structure of matter predicted, that the primary substance is something indeterminate, but it consists of five elements. Four of five elements are terrestrial, namely earth, water, air and fire. The fifth element aether is the heavenly elements[1].

Only the technological advancement, which were achieved in the end of the 19th century and at the beginning of the 20th century allowed to Ernest Rutherford (1871-1937)[1], who is consider as the founder of the nuclear physics, to study the structure of the atoms. Nowadays it is known that fundamental particles of matter are quarks and leptons. A knowledge about these fundamental particles and interaction between them is described by Standard model.

1.1 Quarks and Leptons

Quarks and leptons are fermions that means they have half-integer spin and obey Fermi statistics. Up to the present six quarks are known. They are denoted u, d, c, s, b and t which are respectively, the up, down, charm, strange, bottom (or beauty) and top (or truth). Also six leptons are known. They are electron, electron neutrino, muon, muon neutrino, tau and tau neutrino. Quarks and leptons can be grouped into three generations and every generations contains two quarks and two leptons. The main difference between generations is mass and stability. Higher generation contains particles which have greater mass and are less stable. The up quark with its rest mass about 1.7 - 3.3MeV[2] is the lightest quark. On the other hand, the top quark, which has a rest mass $172.0 \pm 0.9\text{GeV}$ [2], is the heaviest and the least stable quark. The first genera-

tion contains up, down, electron and electron neutrino. The second generation contains charm, strange, muon and muon neutrino. The third generation contains top, bottom, tau and tau neutrino. The overview of all generations can be seen in the Fig. 1.1

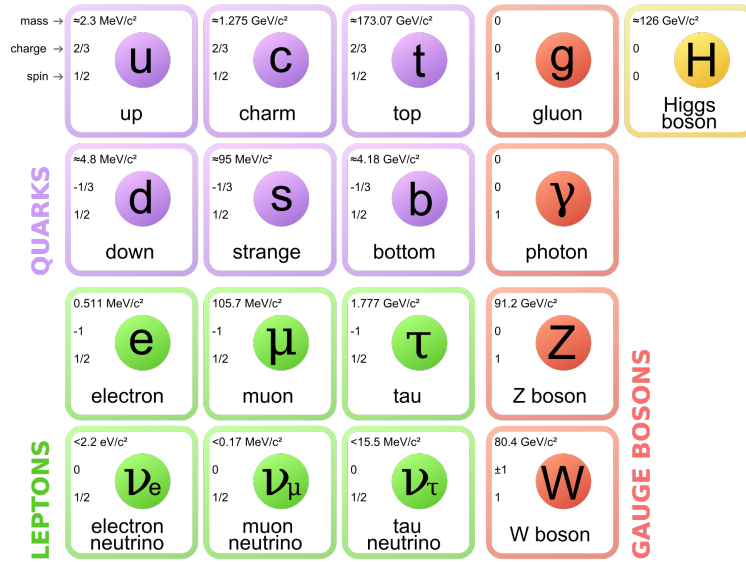


Fig. 1.1: The overview of the quarks, leptons and bosons. Taken from [3].

Quarks are not in nature observed individually, because they are bound into hadrons. Hadrons can be divided into two kinds - baryons and mesons. Baryons are composed of three quarks and mesons are composed of one quark and its antiparticle, antiquark. Baryons have a half-integer spin and obey Fermi-Dirac statistics and mesons are particles with integer spin and obey Bose-Einstein statistics. Hadron can be described by the quantum numbers, e.g. the strangeness, the charm, the topness (or the truth), the bottomness (or the beauty) and baryon number.

All fermions have to follow the Pauli exclusion principle, which claims that in one state two same particle with the same quantum number can not be. For the Pauli exclusion principle to be applicable to all particles, including the particle $\Delta^{++}(uuu)$, $\Delta^-(ddd)$ and $\Omega(sss)$ [2], which as can be seen, consist of three same quarks, another quantum number have to defined. This quantum number is referred as colour, or colour charge. Three values of colour charge were defined (red, blue and green) and relevant to them three types of anti-colour charge (antired, antiblue and antigreen).

1.2 Fundamental interaction

Particle interact between themselves by forces. At the present time four fundamental interactions are known. These fundamental interactions are gravitational, electromagnetic, strong and weak. Each of these interactions can be characterized by the coupling constant, which characterized their strength and by the mediator, which is a particle that is exchanged during their interaction. The carriers of the interaction are the gauge bosons, which in case of electromagnetic, strong, gravitational and weak interactions are photons, gluons, graviton(predicted), bosons W^\pm and Z respectively. These gauge bosons are shown in the Fig. 1.1. There is a brief description of the interaction:

Gravitational interactions

In particle physics the gravitational interaction is neglected, because in comparison with the weak or the strong interaction the strength of gravitational interaction is twenty-five and thirty-eight times respectively smaller.

Electromagnetic interaction

The electromagnetic interaction is the force that acts between charged particles. The range of the electromagnetic interaction is up to the infinity, because the mediator is photon, which has zero mass and photons do not have a charge. To describe this interaction, the quantum electrodynamic (QED) is being used.

Weak interaction

The weak interaction is mediated by exchanged of W^\pm and the neutral charged Z with mass $80.399 \pm 0.023 \text{ GeV}/c^2$ and $91.1876 \pm 0.0021 \text{ GeV}/c^2$ respectively. This mass of the mediators is a reason why the range of this interaction is only about 10^{-3}fm . This force acts between all quarks and leptons. The best known example the weak interaction is beta decay. The weak interaction and electromagnetic interaction was unified into the electroweak interaction in 1970s.

Strong interaction

As the name suggests, the strong interaction is the strongest interaction. The strong interaction acts only between the quarks. Although the gluons, which are the mediators of this interaction, are massless as the photons, the range of the strong interaction is not up to the infinity, but only units of fm. The limitation of the range of the strong interaction is results of the colour charge of gluons. This interaction is describe by the quantum chromodynamics (QCD).

1.2.1 Strong interaction and Asymptotic freedom

The strong potential can be expressed as

$$V(r) = -\frac{4}{3} \frac{\alpha_s}{r} + kr, \quad (1.1)$$

where α_s is the coupling constant, r is a distance between a quark and an anti-quark and k is constant. As can be seen, the first term has a similar behaviour as the Coulomb potential, which for large r tends to zero. The potential for a string, which is the second term, is dominant for large distance, hence the potential energy grows approximately linearly. This shape of the strong potential does not allow quarks to exist individually, but when the potential energy between the quark and antiquark is sufficiently high, the new quark and antiquark can be produced. Subsequently they are bound with the quark and antiquark respectively, thus from one meson develop two mesons.

The strength of the strong interaction can be described by the coupling constant α_s . A theoretical prediction for this coupling constant was made by the physicists David Gross, David Politzer and Frank Wilczek in 1973[4]. They calculated that the coupling constant is function of the momentum transfer q and its behaviour is similar as [4]

$$\alpha_s(q) \sim \frac{1}{\ln \frac{q^2}{\Lambda_{QCD}^2}}, \quad (1.2)$$

where the Λ_{QCD} is a constant. This implies that the coupling constant is small for large momentum transfer and the strength of the strong interaction weakens. This phenomenon is known as the asymptotic freedom[4] and in the region of the asymptotic freedom the perturbative QCD calculation can be used. After experimental verification of their prediction, which can be seen in the Fig.1.2, where the dependence of the coupling constant α_s on an energy is shown, they won the Nobel Prize in Physics 2004 [5].

The asymptotic freedom can be achieved by the decreasing the distance r between the quark and the antiquark. As can be seen from the Eq. 1.3, for small value of r , the dominant term is the first and the second - linear - term can be neglected. The same situation, when the linear term is weakened is by increase temperature of nuclear matter as is shown in Fig.1.3, where can be seen different behaviour of the strong potential for different value of the temperature.

1.3 Quark-gluon plasma

The asymptotic freedom allows a formation of a new state of nuclear matter under extreme conditions in which quarks and gluons are not confined in hadrons can behave almost as free particles. The fact, that they are not absolutely free particles is shown in their collective behaviour. This deconfined state of matter is analogy of plasma, an ionized gas consisting of the free ions and electrons,

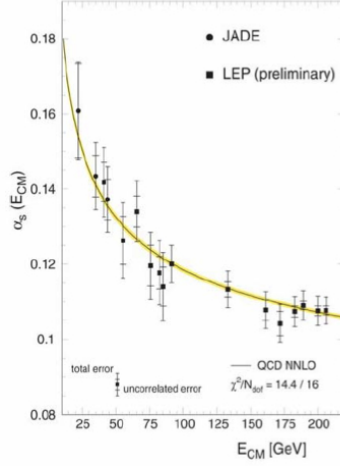


Fig. 1.2: Evolution of the coupling constant α_S as a function of the energy. Taken from [5].

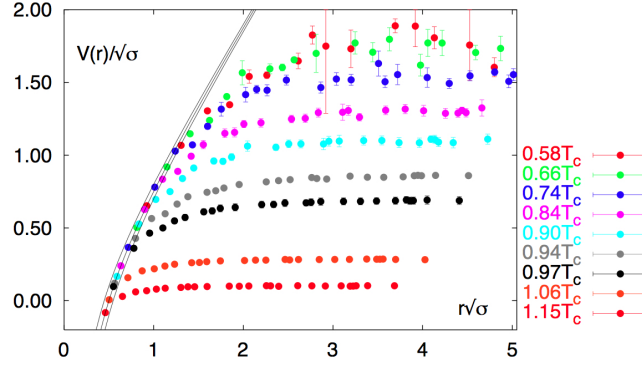


Fig. 1.3: Temperature dependence of the strong potential for different value of the critical temperature. Taken from [6].

which has a collective behaviour. Thus the name of this deconfined matter is the quark-gluon plasma. In the Fig.1.4 it can be seen theoretical prediction the QCD matter phase diagram in the plane of temperature T and baryon chemical potential μ_B , which corresponds to a net baryon density. In the Fig. 1.4 two main states of matter can be seen. In the lower temperature and baryon chemical potential it is hadronic gas and the other state of matter is the Quark-gluon plasma. These two state of matter are divided by the a phase transition line. The phase transition line ends in a critical point E and then it continues at smaller μ_B by a crossover.

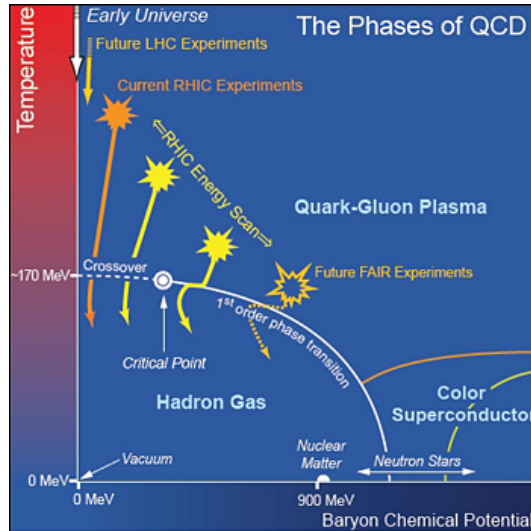


Fig. 1.4: The QCD matter phase diagram. Taken from [7].

To form the quark-gluon plasma, it is necessary to have high temperature and density. On the Earth the only way how to study the quark-gluon plasma is by colliding heavy ions at extreme energies. Heavy ion collision can be studied at experiments which are located e.g. in the Relativistic Heavy Ion Collider (RHIC) at Brookhaven National Laboratory in the USA or in the Large Hadron Collider (LHC) at the European Organization for Nuclear Research (CERN) in Geneva, Switzerland.

In nature these extreme conditions existed few microseconds after the Big bang, which created our universe 13.7 billion years ago. Thus it is assumed that in that time, the quark-gluon plasma existed. This is also one of the motivation for the study of the quark-gluon plasma.

It is assumed that at the beginning of the space-time evolution of the system which is formed after the collision of two heavy ions the quark-gluon plasma can exist. However the system very quickly expands and cools down, and transits back to the confined nuclear matter. The whole evolution ends by emission of particles which are then detected. Hence our information about the formation and existence of the quark-gluon plasma phase is rather indirect. The following signatures [8] can be used for confirmation of the formation of the quark-gluon plasma and for the study of its properties.

1.3.1 Signatures for Quark-gluon plasma

Dilepton production

The quark-gluon plasma contains quarks and antiquarks, which can annihilate and the virtual photon γ^* can be formed. Then this virtual photon decays into a lepton l^- and an antilepton l^+ pair, which can escape from the collision region. Because they interact with other particle only via electromagnetic interaction and it is expected, that their mean-free path is longer than the size of region, which they have to pass through before they leave the collision region. Thus it is unlikely that they will be affected by other particle. According to the fact, that their production depends on the momentum distributions of the quarks and antiquarks, which depends on the thermodynamic condition of the plasma, the dilepton pairs are a good carrier of the information about the conditions inside QGP[8].

On the other hand, the virtual photon, from which the dileptons pair is formed by its decay, can also come from other processes, e.g. Drell-Yan process. By this term is meant process, when valence quark of one nucleon interact with a sea antiquark of the other nucleon from the another nucleus. The result of their interaction is the virtual photon, which decay into the dilepton pair. This process is the main source of the measured background.

Quarkonia suppression

The quarkonia is a bound state of the quark and its antiquark, e.g. J/ψ is bound state of the c quark and \bar{c} antiquark and the Υ is particle consists of the b quark and \bar{b} quark. They are produced in the initial stage of the collision process. When the quarkonia are passing through the collision region, they are influence by the Debye screening, which weakens the interaction between the quark and antiquark pair. The weakening can be so high, that the quarkonia are dissociated into the quark and antiquark, which subsequently interact with lighter quarks or antiquarks and hadronize into open charm mesons. The strength of the dissociation depends on the temperature, thus they can be used for measuring temperature of the source[8].

Photon production

The interaction of the quarks, which are in the quark-gluon plasma with the antiquarks can be describe as[8]

$$\begin{aligned} q + \bar{q} &\rightarrow \gamma + g, \\ q + \bar{q} &\rightarrow \gamma + \gamma. \end{aligned} \tag{1.3}$$

As can be seen, the result of this reaction can be two photons γ , or the photon γ and gluon g . According to the cross section of the interaction, which produced two photons, the most probable is the production of photon and gluon. The formed gluon interacts with the quarks or antiquarks and the photon is

produced. This photon leaves from the collision region and its interaction with other particle is negligible. Because the production of photon and its momentum depends on the quarks and antiquarks, the photons are good carrier information about the thermodynamic condition influencing the quarks and the antiquarks.

Elliptic flow

The elliptic flow[9] is characterized by coefficient v_2 of the second harmonic term in the Fourier expansion of the invariant particle yields

$$\frac{dN_i(b)}{p_T dp_T dy d\varphi_p} = \frac{1}{2\pi} \frac{dN_i(b)}{p_T dp_T dy} [1 + 2v_1^i(p_T, b)\cos\varphi_p + 2v_2^i(p_T, b)\cos(2\varphi_p) + \dots], \quad (1.4)$$

where the b is an impact parameter, p_T is the transverse momentum and φ_b is azimuthal emission angle. The v_2 is sensitive the pressure gradient in the system, which was produced after collision. The largest gradient pressure are in the non-central collision in the direction of the reaction plane.

Nuclear modification factor

The nuclear modification factor is defined as[9]

$$R_{AB}(p_T, y, b) = \frac{d^2 N_{AB}/dydp_T}{\langle T_{AB}(b) \rangle d^2 \sigma_{pp}/dydp_T}, \quad (1.5)$$

where $T_{AB}(b)$ is the Glauber geometrical overlap function of nuclei A,B and the σ_{pp} cross section of proton-proton collision. By the nuclear modification factor, the production of particle in the collision of two nuclei A,B can be compared with the production during the proton-proton collision. In case that the quark-gluon plasma was formed, the production of the particle with higher p_T should be suppressed and the nuclear modification factor is a then smaller than one.

1.4 Nucleus-Nucleus Collisions

The collisions of two nuclei take place at speeds, which are close to speed of light, thus a diameter both nuclei is contracted in the beam direction. This is a reason why nuclei look like a discs. The main parameter used to described the collision of two nuclei is an impact parameter b . This impact parameter b describes how much the nuclei are overlapped in the collision. The impact parameter carries values from 0 to $R_1 + R_2$, where R_1 and R_2 are the radii of the nuclei. The collisions with $b = 0$ are called head-on collisions. On the other hand the collisions with $b \sim R_1 + R_2$ are peripheral collisions. If the impact parameter $0 < b < R_1 + R_2$, the collisions are referred as a semi-peripheral.

Nucleons in collision can be grouped into 2 groups, spectators and participants. The participants, as its name suggests, participate in the collision, thus they have to be located in the overlapping area. The spectators are nucleons,

which do not participate in the collision and after the collision they go on moving. Measuring the number of spectators by "zero-degree calorimeter" is one possible indirect way how to determine the impact parameter. In the Fig. 1.5 the graphic illustration of these terms can be seen.

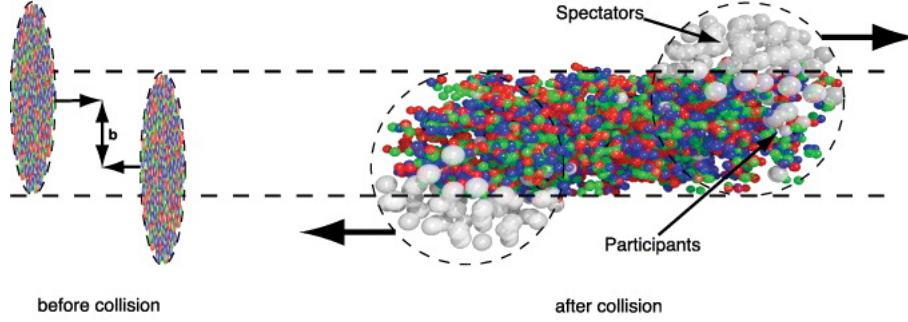


Fig. 1.5: Collision of two nuclei. Taken from [10].

1.4.1 Kinematic Variables

As it was noted the collision of two nuclei take place a place at the speeds, which are closed to the speed of light and very often is necessary to do transition from the one frame to other frame. For this reason it is convenient to use kinematic variables which have simple form under Lorentz transformations [8].

In nucleus-nucleus collisions a particle is characterized by its 4-momentum¹

$$p_\mu = (E, \vec{p}) = (E, p_x, p_y, p_z), \quad (1.6)$$

where E is energy of particle and $\vec{p} = (p_x, p_y, p_z)$ is momentum of particle. In case that a particle is moving in z -direction the momentum of particle can be written as

$$\vec{p} = (p_T, p_L), \quad (1.7)$$

where $p_T = \sqrt{p_x^2 + p_y^2}$ is the transverse momentum which is invariant under Lorentz boost and $p_L = p_z$ is the longitudinal momentum of the particle. Other invariant quantity under Lorentz boost is transverse mass of particle defined as

$$m_T^2 = m^2 + p_T^2, \quad (1.8)$$

where m is rest mass of particle. While velocity is not additive quantity and it is also limited by the value of the speed of the light, the rapidity y , defined as

$$y = \frac{1}{2} \ln \left(\frac{E + p_z}{E - p_z} \right) \quad (1.9)$$

¹The natural units $c=\hbar=1$ are used.

is additive. There is another variable referred as the pseudorapidity η . The pseudorapidity is defined

$$\eta = -\ln \tan \frac{\theta}{2}, \quad (1.10)$$

where $\eta = \arccos \frac{p_z}{p}$. It can be shown, that at very high energy, $p \gg m$ the rapidity equals the pseudorapidity. Because the rapidity can be written in term $y = \frac{1}{2} \ln \left(\frac{E+p_L}{E-p_L} \right) = \frac{1}{2} \ln \left(\frac{\sqrt{m^2+p^2}+p \cos \theta}{\sqrt{m^2+p^2}-p \cos \theta} \right) \approx \frac{1}{2} \ln \left(\frac{p+p \cos \theta}{p-p \cos \theta} \right) = -\ln \tan \frac{\theta}{2} = \eta$. The pseudorapidity is useful, because it is easier to measure an angle θ between the momentum of a particle and a beam axis than a to measure the mass of a particle and its momentum. It means that what that pseudorapidity is defined even when we cannot identify the particle.

1.4.2 Collision evolution

The collision of two nuclei and its evolution is shown in the Fig. 1.6. It is described in one space z and one time t dimension by the space-time diagram. The vertical axis represents the time direction and the horizontal axis represents the spatial direction. The collision of two nuclei occurs at $(t, z) = (0, 0)$ and then the fireball expands going through various processes till the created particles are emitted and detected by the detectors.

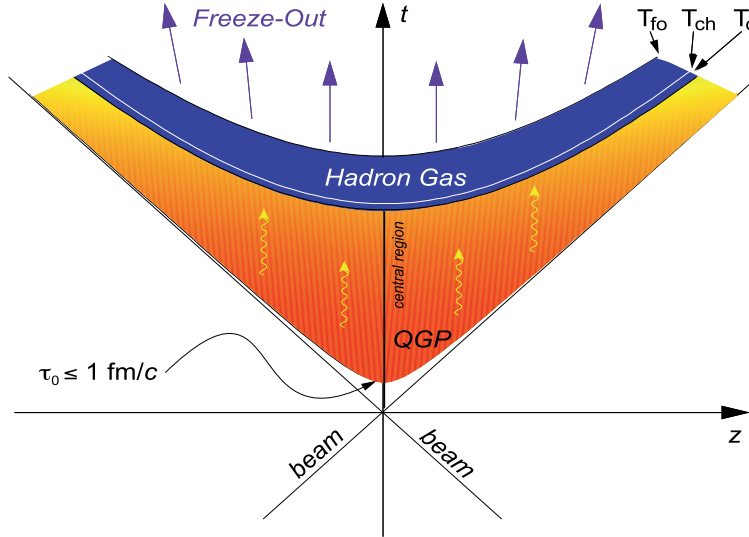


Fig. 1.6: Heavy ion collision. Taken from [11].

There are four main phases of the space-time evolution, namely: pre-equilibrium, Quark-gluon plasma, hadron gas and emitted particles. After the collision, the system is in pre-equilibrium phase. A huge amount of energy is released, each

nucleon scatters several times and there are deconfined quarks and gluons. The pre-equilibrium phase take time $0.1\text{fm}/c < \tau_0 < 1\text{fm}/c$. At time τ_0 the system turns into equilibrium phase - Quark-gluon plasma. According to high pressure, the system expands and the expansion is reason for its cooling. At τ_c the system reaches a critical temperature, in which the Quark-gluon plasma turns into a hadron gas. In this stage of the matter, there is not enough high pressure and density, which allows quarks and gluons to exist deconfined. Hence they have to convert to hadrons. The process of conversion of quarks and gluons into hadrons is called "hadronization". After the hadronization hadrons can continue to scatter and the other particle can be produced. After chemical freeze-out τ_{ch} the amount of hadrons do not change, but they can change their energy due to common interaction by elastic scattering. The ongoing expansion leads to kinematic freeze-out (sometimes it is referred as thermal freeze-out), in which particle stop to interact. Kinematic freeze-out occurs at τ_{fo} and the final phase, in which particle do not interact and they are finally emitted by the source, starts. Emitted particle are then measured by the detector.

Chapter 2

STAR experiment at RHIC

2.1 Relativistic Heavy Ion Collider

The Relativistic Heavy Ion Collider (RHIC)[12] is located at the Brookhaven National Laboratory (BNL) in Upton, New York, USA. It was build to collide the nuclei at relativistic speeds and to study the quark-gluon plasma and the spin structure of the proton. RHIC collides configurations of p+p, Au+Au, d+Au, Cu+Cu and newly U+U. Collisions of these nuclei can achieved maximum energy of beam of $\sqrt{s_{NN}} = 200$ GeV per nucleon and for p+p collision it is $\sqrt{s} = 500$ GeV. The overview of the RHIC runs is shown in the Appendix A, where can be seen the year of the run, the energy of collision and what particle species were collided. Different values of the Au+Au collision energy were used for the Beam energy scan [13]. Its goal was exploration of the quark-gluon plasma boundary and search for a critical point in the phase diagram of the quark-gluon plasma. When RHIC started to operate (June 2000), it had the highest energy of beam, which could be achieve by accelerator on the Earth. But these energies were overcome by the Large Hadron Collider (LHC) in CERN in 2010.

The RHIC is shown in the Fig. 2.1 . The RHIC consists of two independent rings. Circumference of these rings is 3,8km. In these two rings, heavy ions or protons circulate in opposite directions and in places, where the rings intersects, they are collide. There is 6 collision points, but only in 4 places are located detectors. These detectors are called STAR, PHENIX, BRAHMS and PHOBOS. All of these detectors operated from the launch of the RHIC, but nowadays STAR and PHENIX are the only ones operating. BRAMS was stopped in 2006 and PHOBOS stopped in 2005.

Protons and nuclei can not be injected directly into the RHIC, but they have to be preaccelerated by supporting accelerators. After they obtain sufficient energy they can be injected into the RHIC. In the past, the acceleration of nuclei started in the Tandem Van de Graaff accelerator. After they achieved energy of 1MeV, they were sent into the Tandem-to-Booster line and then into

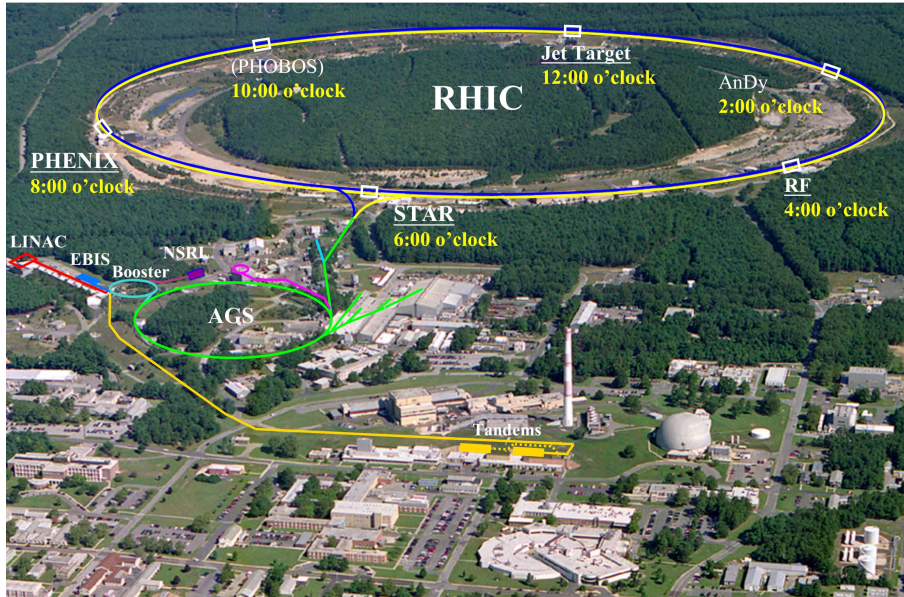


Fig. 2.1: The Relativistic Heavy Ion Collider. Taken from [12].

the Booster Synchrotron, where they were further accelerated and stripped of some electrons. Last step before injection into the RHIC, is an acceleration and stripping of remaining electron in Alternating Gradient Synchrotron (AGS). Acceleration of proton is more simple. They are injected from Linac with energy 200MeV into AGS. And then they continues into the RHIC. But to collide the U+U, it was necessary to do upgrade the supporting accelerators. The Electron Beam Ion Source was installed. This new ion source injects the heavy ions directly into the Booster Synchrotron. [7].

Each detector was constructed and designed for measuring different observables. For this reason, there is difference between construction of detectors. For us, the most important detector is the STAR detector, thus detailed description of the STAR detector can be found in next section and here is brief description of remaining detectors, namely PHOBOS, BRAHMS and PHENIX[14].

PHOBOS detector

The main goal of the PHOBOS[14] detector was to detect all charged particle which were emitted from inelastic collisions. This detector is based on silicon pad detector which consists of a multiplicity array, segmented vertex detector, two small acceptance midrapidity spectrometers, and trigger detectors.

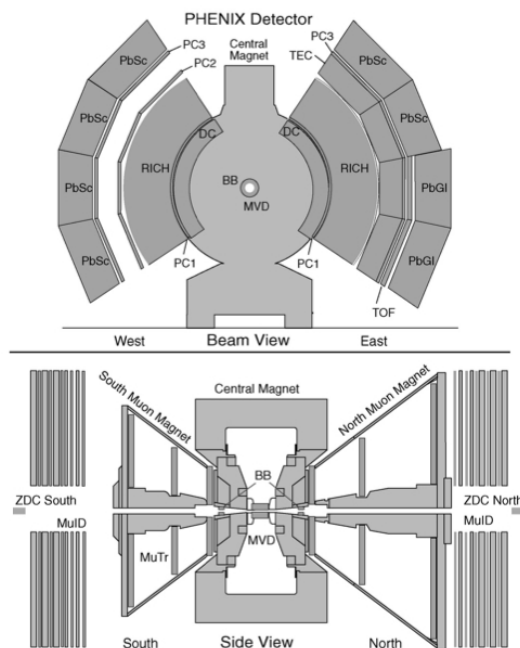


Fig. 2.2: The PHENIX detectors. Taken from [14]

BRAHMS detector

On the other hand, the main goal of the BRAHMS[14] experiment was precise measurements and small angle correlations of primary hadrons. The BRAHMS detector consists of forward scintillator detectors, Zero degree calorimeter, Time Projection Chambers, Cerenkov detectors, Forward spectrometer and midrapidity spectrometer. These spectrometer were used to measure charged particles and their momentum was measured by Time Projection Chamber and Cerenkov detectors.

PHENIX detector

The PHENIX[14] [15] detector, as well as the STAR detector, is still operating. The **P**ioneering **H**igh **E**nergy **N**uclear **I**nteraction **e**Xperiment is able to measure many observables and signals, especially direct photons, lepton pairs, J/ψ and Υ particles. The PHENIX detector is shown in Fig. 2.2 and it contains many sub detectors namely: four spectrometers, Time of Flight, Ring Imaging Cerenkov and Time Expansion Chamber detectors.

2.2 STAR detector

The Solenoid Tracker At RHIC[16] is multi-purpose detector. It covers an azimuthal angle $0 < \phi < 2\pi$ and it is able to measure in pseudorapidity up to $|\eta| < 1.8$. It consists of many subdetectors and systems, which are shown in Fig. 2.3. The main subdetectors and systems are the Time Projection Chamber (TPC), the Time Of Flight (TOF), the Barrel Electromagnetic Calorimeter (BEMC), the Endcap Electromagnetic Calorimeter (EEMC), the Beam-Beam Counter (BBC), the Photon Multiplicity detector (PHD), the Forward Pion detector (FPD), the primary Vertex Position detector (pVPD), the Zero Degree Calorimeter (ZDC)[16]. Other important system is a magnet. It has shape of tube and it is 6.85 meter long and its outer radius is 7.32 meter. It can produce a uniform magnetic field of 0,5 T [16].

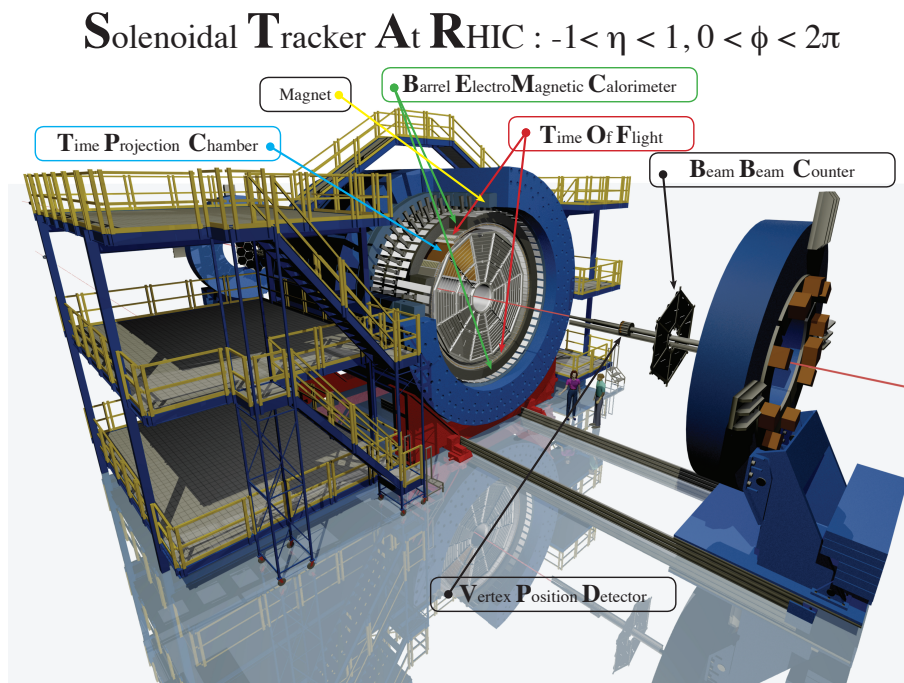


Fig. 2.3: The STAR detector. Taken from [12] .

2.2.1 Time Projection Chamber

The Time Projection Chamber (TPC)[17] is the main detector of the STAR. It covers full azimuthal angle and pseudorapidity up to $|\eta| < 1$. Its main purpose is the reconstruction of particles trajectory and identification of charged particles

by measuring their energy loss and curvature of their trajectory in the magnetic field.

As can be seen from Fig. 2.4 , the TPC is divided by High Voltage Membrane at the centre of the TPC. Typical potential at High Voltage Membrane is 28kV. Inside of TPC is then a uniform electric field of 135V/cm. The TPC is filled by gas P10 which a is mixture of argon (90%) and methane (10%) and its pressure is 2 mbar higher than atmospheric pressure. Particles, which pass through the gas, ionize this gas creating free electrons and ions. Ions travel in electric field to cathode (High Voltage Membrana) and electrons go to the anode. Electron motion to anode is not direct, because they collide with other atoms of gas and their velocity is not constant. For this reason, a drift velocity is defined as average velocity and in the TPC their drift velocity is 5.45 cm/ μ s.

At each end of the TPC is a readout system based on Multi-Wire Proportional Chambers with readout pads. There are altogether 12 anode pads. Each anode pad (see Fig. 2.5) is divided into inner subsection and outer subsection. Inner subsection contains 1,750 pads and outer subsection contains 3,942 pads. Thus the total number of pads is 136,608. These pads record electrons coming from the gas ionized by traversing particles. Before the anode there is so strong electric field, thus the electrons can further ionize the gas. This is know as avalanche effect[17]. The main advantage of avalanche effect is that the signal is 1000-3000 times amplified.

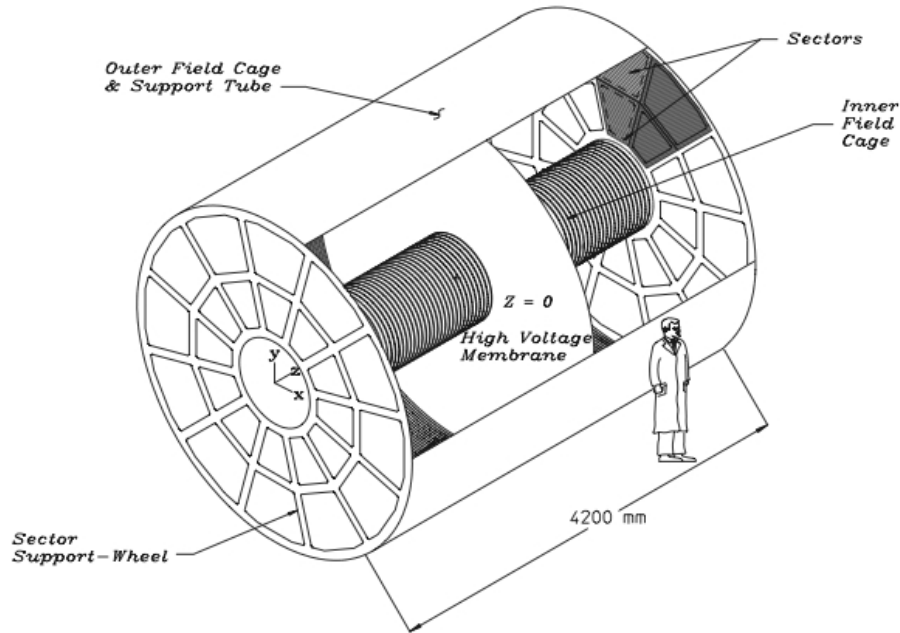


Fig. 2.4: The Time Projection Chamber. Taken from [17] .

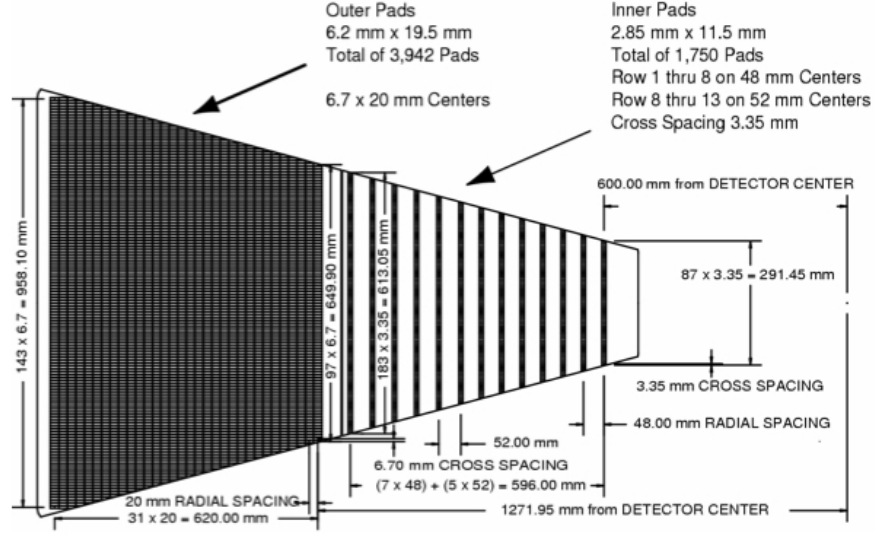


Fig. 2.5: The anode pad. Taken from [17] .

To reconstruct the trajectory of a particle, coordinates (x,y,z) have to be known. The coordinates (x,y) are determined by the pads, which were stricken by electrons. The coordinators (z) is calculated from the knowledge of drift velocity and drift time.

Particles traversing the TPC loose energy mainly by ionization(they can loss energy by radiation, but this is neglected). The energy loss can be calculated by using Bichsel function[18], which is modified Bethe-Bloch function[18]. Formula for Bichsel function is

$$\left\langle -\frac{dE}{dx} \right\rangle = 2\pi N_A r_e^2 m c^2 \rho \frac{Z}{A} \frac{z^2}{\beta^2} \left[\ln \left(\frac{2mc^2 \gamma^2 \beta^2 W_{MAX}}{I^2} \right) - \beta^2 - \frac{\delta^2}{2} \right], \quad (2.1)$$

where N_A is Avogadro's number, r_e is classical electron radius, m is mass of particle, c is speed of light in vacuum, ρ is density of material, Z and A are atomic number and weight of material, W_{MAX} is maximum energy transfer in a single collision, I is mean excitation energy, δ is density correction.

Thus ionisation energy loss $\left\langle -\frac{dE}{dx} \right\rangle$ can be function of momentum of particles. In Fig. 2.7 is shown $\frac{dE}{dx}$ as a function of momentum of particles from the STAR TPC. As can be seen the TPC allows to separate pions and kaons with momentum up to 0.6 GeV/c [17]. This method of identification is suitable, but of course, it has some limits. It can be problem for region, where curves $\left\langle -\frac{dE}{dx} \right\rangle$ of different particles overlap. Other problem is for particles with high transverse momentum, because there is a relativistic rise in region, where function $\left\langle -\frac{dE}{dx} \right\rangle$ flatten. For better identification the Time Of Flight detector have to be used.

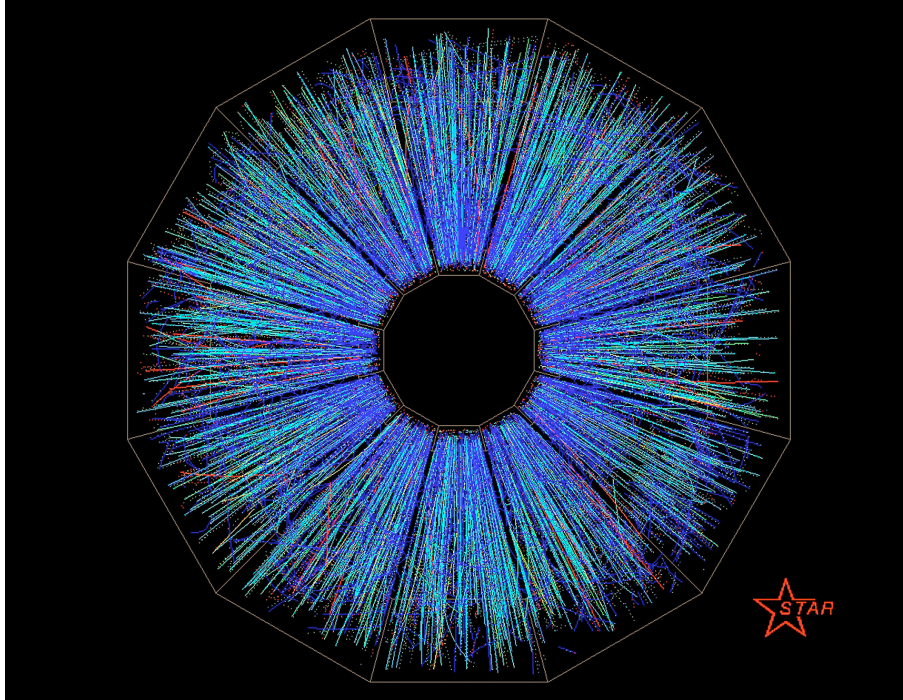


Fig. 2.6: The trajectories of particles, which was reconstructed by using TPC. Taken from [12] .

2.2.2 Time Of Flight detector

The main function of the Time of Flight detector (TOF)[20], as its name suggests, is a precise measure the time of flight of particles. With measured time Δt , which particle needed to pass known distance Δs , the inverse velocity $\frac{1}{\beta}$ is calculated as

$$\frac{c}{v} = \frac{1}{\beta} = c \frac{\Delta t}{\Delta s}. \quad (2.2)$$

This $\Delta t = t_2 - t_1$ is measured by TOF, respectively the TOF measured t_2 . t_1 is measured by other subdetector, which is called primary Vertex Position detectors (pVPD). The inverse velocity is used to calculated the mass of particle. The mass of particle can be calculated as

$$m = \frac{p}{\beta\gamma c} = \frac{p\sqrt{1-\beta^2}}{\beta c} = \frac{p}{c} \sqrt{\frac{1}{\beta^2} - 1}. \quad (2.3)$$

The TOF, which was installed in STAR in 2010, covers pseudorapidity $|\eta| < 1$ and full azimuthal angle . This detectors is based on Multi-gap Resistive Plate Chamber (MRPC) technology and its time resolution is about 87ps. This high

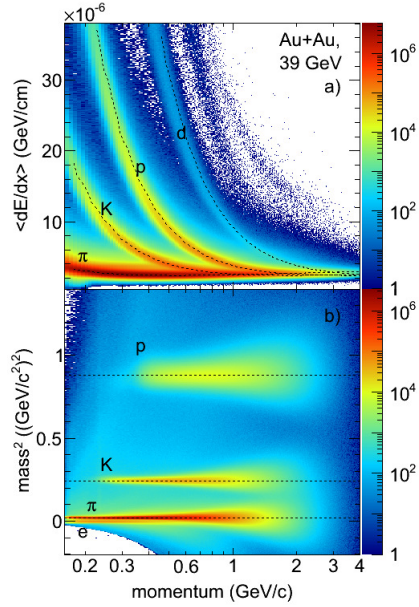


Fig. 2.7: Result from measuring dE/dx . Taken from [19] .

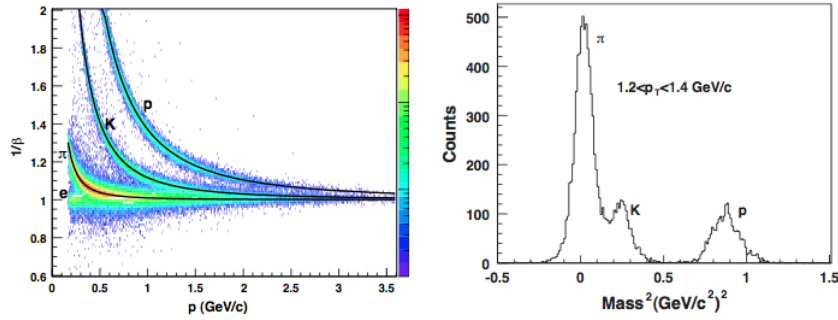


Fig. 2.8: Result from data analysis from the TOF. Taken from [21] .

resolution allows the TOF to distinguish between electrons with the momentum up to 1.5 GeV/c and heavy hadrons at low momentum, like kaons and protons. Fig. 2.8 shows results from data analysis from the TOF.

2.2.3 Barrel Electromagnetic Calorimeter

The Barrel Electromagnetic Calorimeter (BEMC) [22] is sampling a calorimeter, which is situated between the TOF and the magnet. From the beam pipe, the BEMC is at a distance of 223.5 cm. The BEMC, as well as the TOF and the TPC, covers the pseudorapidity $|\eta| < 1$ and full azimuthal angle. It is used to measure energy of high energy electrons and photons as well to identify electrons in dense hadronic background. The BEMC can also identify neutral pions via their decay into two photons at high transverse momentum $p_T = 25 - 30 \text{ GeV}/c$. The BEMC consists of 120 calorimeter modules and each module is divided into 40 towers, 2 towers are in ϕ - direction and 20 towers are in η - direction. Each module (see the Fig.2.9) is made of 21 active scintillating layers and between them there are lead absorber plates and other components (Detailed description can be found in [22]).

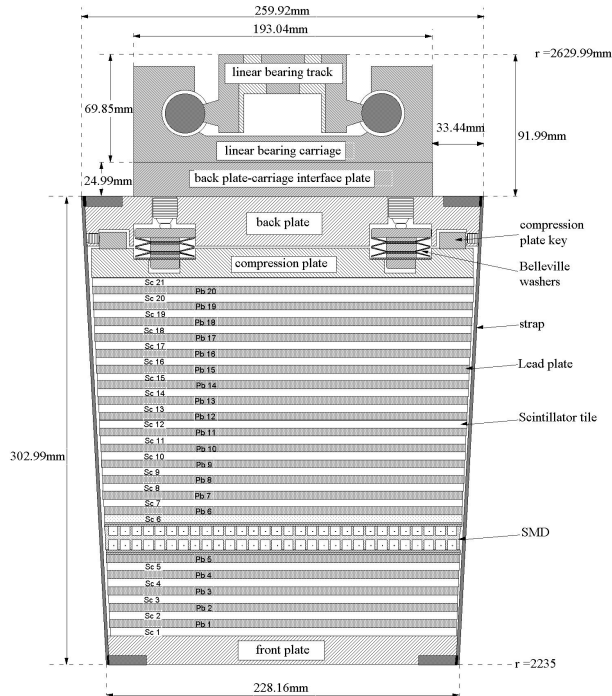


Fig. 2.9: The view of BEMC module. Taken from [22] .

The function of active scintillating layers is to measure part of the energy deposited by the traversing charged particle which is lost due to Bremsstrahlung inside of the scintillator. From this information we can deduce the energy deposited by the particle in the whole calorimeter. The actual amount of the deposited energy in the whole calorimeter depends on the type of particle. For electron the thickness of the detector corresponds to 20 radiation lengths. The

radiation length is defined as a length, which particle has to pass to lose to $1/e$ of its original energy. Hence the electrons and photons are expected to be fully stopped in the calorimeter. On the other hand, hadrons have smaller interaction cross section with the lead. This is a reason, why they pass through the calorimeters as minimum ionizing particles and they do not deposit their whole energy. This fact can be used to identify electrons in the calorimeter. For electrons with momentum of units of MeV and higher, their mass can be neglected and their deposited energy is almost equal to their momentum. Their energy-to-momentum ratio is hence $E/p \sim 1$ while for hadrons the deposited energy is smaller and their E/p will decrease with increasing p . At STAR this is the main way, how to identify electrons with high momentum $p \geq 1.5 GeV$.

2.3 STAR trigger system

During data taking of typical Au+Au collisions at $\sqrt{s_{NN}}=200$ GeV collision rate delivered by the RHIC accelerator for STAR experiment is 50kHz. It is technically impossible to record and analyze all events, because the speed at which detectors operate is of an order lower. It is also not necessary to analyze every event.

The rate of readout has to be reduced and for this purpose a trigger systems[23] is being used. The STAR trigger system consists of four levels - Level 0, Level 1, Level 2 and Level 3. The Trigger system uses information from the fast detectors and based on this information it makes decision whether to record given event. The fast detectors are the ZDC, the pVPD, the BBC, the EEMC, the TOF and the BEMC. The Level 0 trigger monitors each collision and determines whether there is a collision which fulfills our requirements. The Level 0 uses the pVPD, the ZDC and the BBC. The ZDC is also able to monitor the luminosity. With knowledge of number spectators, the centrality of collision can be detected. For head-on collision there would be a minimal number of spectators. On the other hand, the peripheral collisions have a huge amount of spectators. This principle allows to use ZDC for triggering on the centrality of event.

When the Level 0 completed its analysis and did not abort the readout, the Level 1 and 2 can start. Analysis from the Level 1 and the Level 2 is more complex and it takes more time. The Level 2 takes about 5ms. In comparison with the Level 0, which takes only $1,5\mu s$, the Level 2 take a "very long" time. The final Level 3 is an online analysis done by CPU farms. Based on its results a decision is made whether event will be stored by the DAQ[24].

The STAR detectors produce data and its rate is up to 8,000MB/s. The STAR Data Acquisition System (DAQ) is responsible for readout these data from detectors, reducing them and storing data into a storage, which uses a tape based High Performance Storage Systems (HPSS). After the last upgrade in 2009, the DAQ operates with the rate of 1kHz.

2.4 On-going upgrade of the STAR detectors

Currently there is two main detectors, the Muon Telescope Detector and the Heavy Flavor Tracker, which are being installed into the STAR detectors.

2.4.1 Muon Telescope Detector

The reason, why the Muon Telescope detector (MTD)[25] is being installed, is to enable detection of muons. The muons are more penetrating than e.g. electrons. Hence they are not stopped in the lead absorber plates in the BEMC nor in the magnet, which can stops all other particles. The muons penetrate through the BEMC and the magnet and then will be detected by the MTD, which is situated behind the magnet.

The muons can originate from Quark-gluon plasma thermal radiation, J/ψ , quarkonia, light vector mesons, semi-leptonic decays etc. In cooperation with other detectors the MTD provides good mass resolution for measurements of vector mesons and quarkonia. It is able to distinguish different state of Υ . The MTD covers 45% of azimuthal angle and pseudo rapidity $|\eta| < 0.5$ and its radius is ~ 400 cm. It consists of the same electronics as the TOF and it works with timing, which will be smaller than 100ps and its spacial resolution is 1 cm.

2.4.2 Heavy Flavor Tracker

Other detector, which is was prepared to install, is the Heavy Flavor Tracker (HFT)[26]. The HFT is a silicon vertex, which replacing silicon drift detector (SVT) and it is the first vertex detector, which using CMOS active pixel sensor technology. The HFT makes it possible to study heavy flavour production,



Fig. 2.10: The schema of Heavy Flavor Tracker. Taken from [27] .

because it is able to measure the charmed mesons decays such as D^+ , $D^- \dots$ containing charm quark[27]. The HFT(see Fig. 2.10) consists of two layers of silicon detector. The inner layers of silicon detector is only 1.5 cm from the beam pipe and it is composed of 6 detector ladders. The outer layers is at distance of 5 cm from the beam pipe and it is made of 18 detector ladders. In

order situate the new detector so close to the beam pipe it is necessary to make radius of the beam pipe thinner.

2.5 Future of the STAR detector

By installing the HFT and the MTD, the upgrade of the STAR detector does not end. There will be Beam Energy Scan II program, p+A program, which will allow to study collisions of polarized protons with nuclei. However the main upgrade, which is planned on 2020-2025 timescale is referred as eRHIC. The eRHIC (see Fig. 3.7) will be electron ion collider, which will be made by rebuilding the RHIC. The main purpose of the eRHIC will be the study electron-ion or electron-proton collision. A top energy, which ion will have, should be 100GeV, 250GeV for proton respectively.

The eRHIC[28] program will need to upgrade all detectors and will use new technologies which are now under development. For example a polarised electron gun, strong hadron beam cooling, which will be based on a Coherent electron Cooling (CeC), a multi-pass Energy Recovery Linac (ERL) etc. The ERL will be used as an electron accelerator, which will be located inside the RHIC tunnel. The energy of electron from this accelerator will be up to 30GeV.

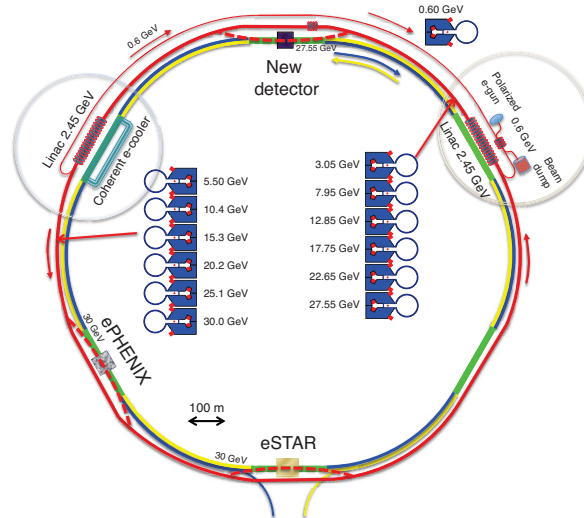


Fig. 2.11: The eRHIC. Taken from [28] .

Chapter 3

Correlation femtoscopy

3.1 Historical background of femtoscopy

A technique, which is used to study the space-time structure and allows to determine source size at freeze-out is referred as femtoscopy. It is sometimes also called HBT as a reference to authors of this technique.

In 1950's Robert Hanbury Brown and Richard Q. Twiss developed this technique and used it to measure the angular size of stellar objects. At first they used for their measurements Sun and then with high precision they measured the angular size of Sirius star [29]. They chose Sirius, because it is the brightest star in the night sky. The principle of their technique was to use the photon intensity interferometry. It was alternative to measurement, which was based on amplitude interferometry of Michelson.

First application of femtoscopy in particle physics was in 1960's by G. Goldhaber, S. Goldhaber, W.-Y. Lee and A. Pais [30]. They paid attention to reaction of the annihilation of proton and anti-proton.

$$\bar{p} + p \rightarrow \pi^{\pm} + \pi^{\pm} + n\pi^0 + \dots \quad (3.1)$$

They studied production of pion pairs and their angular distribution. They observed enhancement of $\pi^-\pi^-$ and $\pi^+\pi^+$ pairs at low relative momentum. They also correctly asserted that this correlation comes from a quantum statistics. The results of their measurement can be seen in the Fig. 3.3. However, the main share of developing the femtoscopy is owned by Russian scientists and mathematicians G. I. Kopylov and M. I. Podgoretsky, who developed mathematical formalism for this method.

3.2 Correlation function

For a description of the main principle of correlation femtoscopy the Fig. 3.2 is used. As can be seen from the Fig.3.2 there is a source, which emitted two particles with 4-momentum p_1, p_2 from x_1, x_2 respectively. The single-particle

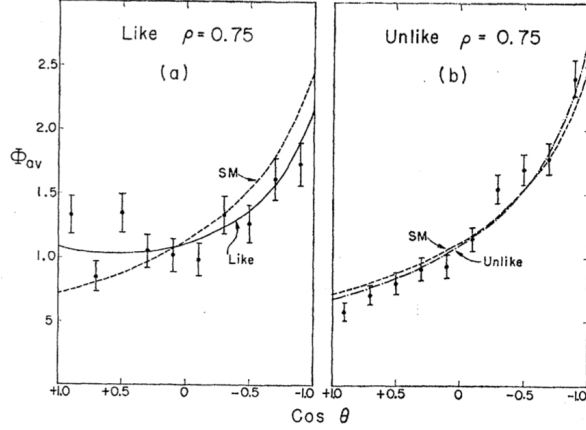


Fig. 3.1: The result of measurement of enhancement of $\pi^-\pi^-$ and $\pi^+\pi^+$ pairs. Taken from [30].

source can be characterized by an emission function $S(x, p)$. The emission function can be understood as a probability of emission of particle with 4-momentum p from x . Thus the total probability of emission of particle is the integral over the whole source

$$P(\vec{p}) = \int d^4x S(x, p). \quad (3.2)$$

This is for emission of one particle. For two independent particles, the probability of emission of two particles with 4-momentum p_1, p_2 from x_1, x_2 is

$$P(\vec{p}_1, \vec{p}_2) = \int d^4x_1 d^4x_2 S(x_1, p_1) S(x_2, p_2) = \int d^4x_1 S(x_1, p_1) \int d^4x_2 S(x_2, p_2). \quad (3.3)$$

However the emitted particles interact between themselves and its interaction is described by a wave function. The calculation of probability of emission of two interacting particles has to contain this wave function, thus the probability is given by a term

$$P(\vec{p}_1, \vec{p}_2) = \int d^4x_1 d^4x_2 S(x_1, p_1) S(x_2, p_2) |\psi|^2 \quad (3.4)$$

where ψ is a wave function, which described interaction of two particles. The simplest possible case on which technique will be demonstrated is for identical and non-interaction particles. The wave function, which is used for this simplest case and is constructed only by a knowledge of quantum statistics¹ is

$$\psi = \frac{1}{\sqrt{2}} \left[e^{i(x_1' - x_1)p_1} e^{i(x_2' - x_2)p_2} \pm e^{i(x_1' - x_2)p_1} e^{i(x_2' - x_1)p_2} \right]. \quad (3.5)$$

¹Bose-Einstein statistics for bosons and Fermi-Dirac statistics for fermions

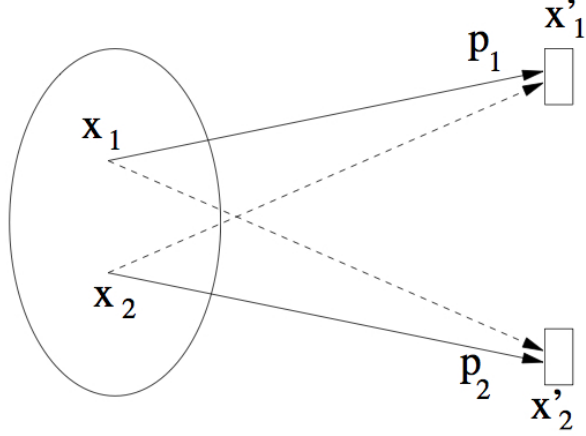


Fig. 3.2: The schema of emission of particle. Taken from [31] .

Because the particles are indistinguishable, there is no chance to say certainly, that the particle, which was emitted from x_1 is detected in x'_1 . This particle can be detected in x'_2 and in x'_1 the particle from x_2 can be detected. For this reason, the wave function has to be symmetrized or anti-symmetrized. The symmetrized wave function (sign +) is for bosons and the anti-symmetrized wave function (sign -) is for fermions. The final state interactions make the wave function more complicated and here is an example: if the charged particles are used, the Coulomb interaction has to be considered and the relative wave function for description this interaction [32] is

$$\phi = \Gamma(1 + i\eta) e^{-\pi\eta/2} e^{iqr} \left\{ 1 + \sum_{n=1}^{\infty} h_n (r/a_0)^n \right\}, \quad (3.6)$$

where a_0 is the Bohr radius, $\eta \equiv \mu e^2 / \hbar q$, $h_1 = 1$ and $h_n = \frac{n-1-i\eta}{-i\eta n} h_{n-1}$. The calculation with this wave function needs a deeper understanding of a quantum mechanics, which is used for calculations with this wave function. Using it is unfortunately beyond the scope of this bachelor thesis. The squared the wave function from the Eq. 3.5 is

$$|\psi|^2 = \psi\psi^* = \frac{1}{2} (2 \pm 2 \cos((\vec{p}_1 - \vec{p}_2) \cdot (\vec{x}_1 - \vec{x}_2))) = 1 \pm \cos((\vec{p}_1 - \vec{p}_2) \cdot (\vec{x}_1 - \vec{x}_2)). \quad (3.7)$$

Let us introduce the relative pair momentum as

$$q = p_1 - p_2 \quad (3.8)$$

and average pair momentum as

$$K = \frac{p_1 + p_2}{2} = \frac{P}{2}. \quad (3.9)$$

As it will be seen subsequently it is suitable to transform x_1 and x_2 into variables r and x defined as

$$r = x_1 - x_2, \quad (3.10)$$

$$x = \frac{1}{2}(x_1 + x_2) \quad (3.11)$$

respectively. By these variables, the terms for x_1 and x_2 are

$$x_1 = x + \frac{r}{2}, \quad (3.12)$$

$$x_2 = x - \frac{r}{2}. \quad (3.13)$$

By using these relations (the Eq. 3.10 and the Eq. 3.8) the Eq. 3.7 can be rewritten into form

$$|\psi|^2 = 1 \pm \cos(\vec{q} \cdot \vec{r}). \quad (3.14)$$

Experimentally the two particle correlation function can be constructed as the ratio of the measured two particle inclusive spectra and single-particle inclusive spectra [32] i.e.

$$C(\vec{P}, \vec{q}) = \frac{dN^{12}/(d^3p_1 d^3p_2)}{(dN^1/d^3p_1)(dN^2/d^3p_2)}. \quad (3.15)$$

This expression has the same meaning like the correlation function would be defined as a ratio of the probability of emission of two interacting particle and the probability of emission each particle. Assuming that the Eq. 3.2 and the Eq. 3.5 are used, the definition of the correlation function can be mathematically written as

$$\begin{aligned} C(\vec{P}, \vec{q}) &= \frac{dN^{12}/(d^3p_1 d^3p_2)}{(dN^1/d^3p_1)(dN^2/d^3p_2)} = \frac{P(\vec{p}_1, \vec{p}_2)}{P(\vec{p}_1)P(\vec{p}_2)} = \\ &= \frac{\int d^4x_1 d^4x_2 S(x_1, p_1) S(x_2, p_2) |\psi(\vec{q}, \vec{r})|^2}{\int d^4x_1 S(x_1, p_1) \int d^4x_2 S(x_2, p_2)}. \end{aligned} \quad (3.16)$$

The application of the result from the Eq.3.14 leads to

$$C(\vec{P}, \vec{q}) = 1 \pm \frac{\int d^4x_1 S(x_1, p_1) d^4x_2 S(x_2, p_2) \cos(\vec{q} \cdot \vec{r})}{\int d^4x_1 S(x_1, p_1) \int d^4x_2 S(x_2, p_2)}. \quad (3.17)$$

If the Eq.3.9, Eq.3.8, Eq.3.12 and Eq.3.13 are used, the numerator from the fraction in the Eq.3.17 can be expressed as

$$\begin{aligned} &\int d^4x_1 S(x_1, p_1) d^4x_2 S(x_2, p_2) \cos(\vec{q} \cdot \vec{r}) = \\ &= \int d^4x d^4r S\left(x + \frac{r}{2}, K + \frac{q}{2}\right) S\left(x - \frac{r}{2}, K - \frac{q}{2}\right) \cos(\vec{q} \cdot \vec{r}) \stackrel{1}{\approx} \\ &\stackrel{1}{\approx} \int d^4x d^4r S\left(x + \frac{r}{2}, K\right) S\left(x - \frac{r}{2}, K\right) \cos(\vec{q} \cdot \vec{r}) = \\ &= \int d^4r \cos(\vec{q} \cdot \vec{r}) \int d^4x S\left(x + \frac{r}{2}, K\right) S\left(x - \frac{r}{2}, K\right). \end{aligned} \quad (3.18)$$

The approximation noted \approx^1 , when the relative pair momentum is neglected is called "the smoothness approximation" and it is valid for small relative momenta. The expression $\int d^4x S(x + \frac{r}{2}, K) S(x - \frac{r}{2}, K)$ is the function of r and K , thus it can be rewritten as $d(r, K)$ and it is referred as the *relative distance distribution*. It should be noted that the relative distance distribution is an even function of r . After modifying the denominator term in the same way, the correlation function will be expressed as

$$\begin{aligned} C(\vec{P}, \vec{q}) &= 1 \pm \frac{\int d^4r \cos(\vec{q} \cdot \vec{r}) d(r, K)}{|\int d^4x S(x, K)|^2} = 1 \pm \frac{\int d^3r \cos(\vec{q} \cdot \vec{r}) \int dt d(\vec{r} + \vec{\beta}t, K)}{|\int d^4x S(x, K)|^2} = \\ &= 1 \pm \frac{\int d^3r \cos(\vec{q} \cdot \vec{r}) S_{\vec{K}}(\vec{r})}{|\int d^4x S(x, K)|^2}, \end{aligned} \quad (3.19)$$

where $S_{\vec{K}}(\vec{r}) = \int dt d(\vec{r} + \vec{\beta}t, K)$ is the *relative source function*. The last alteration was done due to the fact, that two particles are on-shell thus the four components of q are not independent, but related by

$$q^0 = \vec{\beta} \cdot \vec{q}, \quad (3.20)$$

where

$$\vec{\beta} = \frac{\vec{K}}{K_0} \approx \frac{\vec{K}}{E_k}. \quad (3.21)$$

This on-shell approximation allows to rewritten the integrand in Eq.3.19 and obtained the relative source function $S_{\vec{K}}(\vec{r})$. Thus as can be seen, the Fourier transform in Eq.3.19 is therefore not invertible and the reconstruction of the space-time structure of the source will always require additional model assumptions.

This is one of possible way, how to derive the formula for the two-particle correlation function. In another literature [33] can be found this expression

$$C(\vec{q}, \vec{K}) = 1 \pm \frac{|\int d^4r S(r, K) e^{iqr}|^2}{\int d^4x_1 S(x_1, K + \frac{q}{2}) \int d^4x_2 S(x_2, K - \frac{q}{2})}, \quad (3.22)$$

which is the function of the relative and average momenta of the pair particle and the numerator is just the 3-dimensional Fourier transform of the emission function in variables x . This definition was obtained from the solution of the Klein-Gordon equation [32], which needs relativistic quantum treating, which is beyond of my knowledge of quantum mechanics.

This definition of the correlation function can be still simplified in case for which the smoothness approximation is applicable. The simplest expression for the correlation function is then

$$C(\vec{q}, \vec{K}) = 1 \pm \frac{|\int d^4r S(r, K) e^{iqr}|^2}{|\int d^4x S(x, K)|^2}, \quad (3.23)$$

where the denominator is the normalization condition. Thus for the normalization emission function

$$s(r, K) = \frac{S(r, K)}{\int d^4x S(x, K)} \quad (3.24)$$

the term is converted into

$$C(\vec{q}, \vec{K}) = 1 \pm \left| \int d^4r s(r, K) e^{iqr} \right|^2. \quad (3.25)$$

Due to the fact, that q have only 3 independent components, the Eq.3.25 is not the 4-dimensional Fourier transform, how it could look like. The time component cannot be unambiguously reconstructed. The time information is convoluted into the relative distance distribution function. Thus the Fourier transform is not invertible and the time-structure of the source can be studied by comparison with model describing 4-dimensional particle emission.

As can be seen from the deriving the correlation function, it consists of the relative source function and the wave function. Up to now, someone could think, that the correlation femtoscopy is used only to study the space-time structure of the particle source. But it is not the only possible use of the correlation function. It can be also used to study the interaction between particle, which is described by the wave function. If the source distribution is known or assumed and the correlation function is experimentally obtained then new information about the interaction of emitted particle can be extracted.

3.3 Coordinate Systems

Choice of the coordinate systems is very important, because suitable choice can make working with the correlation function easier. On the other hand badly or inappropriate selection of the coordinate system can tend to that the further calculation will be more complicated or even impossible. During the choosing the coordinate systems all symmetries and using variables should be considered. The correlation function depends on \vec{q} and \vec{P}, \vec{K} respectively - variables determine by momentum of measured particles. This simple fact should affect the choice of the coordinate system or at least one of main axis.

The Bertsch-Pratt coordinate system [32] (shown in Fig.3.3), which is often being used, looks like the most appropriate for the correlation femtoscopy. In comparison with the laboratory system the main directions of axis are given by momentum of the observed pair. It is usually noted as "out-side-long" system as references to the directions of axes, by which the coordinate system is characterized. This system is described by three main Cartesian axis - namely: longitudinal, outward and sideward axis. The longitudinal axis is parallel to the beam - typical in laboratory system z -axis. The direction of the outward axis is determined by previously mentioned momentum of emitted particle, because the outward axis is parallel to pair transverse momentum P_T . The last axis - the sideward axis - is chosen so that it would be perpendicular to the longitudinal and outward axes. The way of defining of the outward axis causes that

each pair of particles is described in different "out-side-long" system, because the coordinate system is connected with the emitted pair. In this coordinate system each four vector V has these components:

$$\begin{aligned} V_{long} &= V_z \\ V_{out} &= (P_x V_x + P_y V_y) / P_T \\ V_{side} &= (P_x V_y - P_y V_x) / P_T \end{aligned} \quad (3.26)$$

where are project out by $P = (P_0, P_x, P_y, P_z)$.

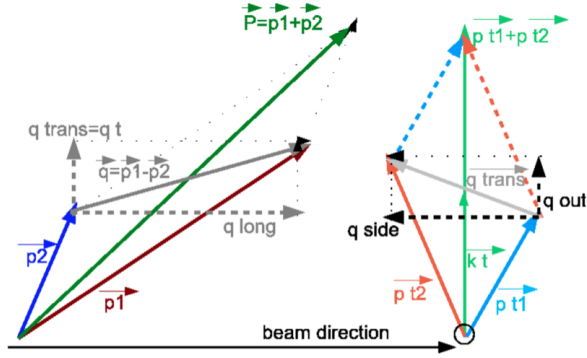


Fig. 3.3: The Bertsch-Pratt coordinate system. Taken from [34] .

Instead of laboratory frame the femtoscopic analysis commonly used the longitudinally co-moving system (LCMS). This system moves along the beam direction with the same velocity thus in the LCMS $P_z = 0$. Its three main axes are chosen according to the "out-side-long" system. This choice of coordinate system eliminates the effects due to longitudinal expansion of the system.

In case of study of the interacting particles, it is suitable use the pair's rest frame (PRF). In this frame particles move only away from each other. PRF is commonly used for non-identical particle, where the construction of the wave function of this pair is hard and sometimes can be constructed only in the PRF. The relative pair momentum is noted as

$$\vec{q} = 2\vec{k}^*, \quad (3.27)$$

where each particle have the same momentum $\vec{k}^* = \vec{k}_1 = -\vec{k}_2$, where the subscript 1 and 2 noted the first and second particle respectively. The symbol * refers to the PRF.

3.4 Parametrization of correlation function

After the choice of the coordinate system the next step, which helps us to gain information about the space-time structure of the source from the correlation

function is a parametrization. The correlation function and the relative source function is usually parametrized by Gaussians [32]. Although it is known, that the resonance decay contributions can cause the exponential tails, which tends to the fact, that the realistic source deviate from Gaussians. On the one hand using the parametrization, which would be a little different from the Gaussian and could describe this deviate would be helpful, but the fitting would be more complicated. One of a reason, why in the practice the Gaussians is used is the fact, that the fluctuations of measured variables leads to Gaussian. In addition to it, Fourier transform of Gaussian is Gaussian, which is useful in the case of non-interaction identical particle, where the wave function is constructed by knowledge of a quantum statistics (see Eq. 3.25).

Usually, the simplest case is one-dimensional, in which case the correlation function is parametrized [31] as

$$C(\vec{q}, \vec{K}) = 1 + \lambda(\vec{K}) \exp\left(-Q_{inv}^2 R_{inv}^2(\vec{K})\right), \quad (3.28)$$

where the λ factor, the R_{inv} parameter and $Q_{inv}^2 = -q^2$, which is defined as $q = \sqrt{(E_1 - E_2)^2 - (p_1 - p_2)^2}$ are used. The λ factor or parameter is sometimes called as the incoherence factor. This factor was defined, because the measured correlation function was smaller than the theoretical prediction and the λ factor compensates this difference which can be caused by the misidentified particle or by the particles, which come from long-lived resonance, where any correlation can not be observed. To sum up, the λ factor compensates all inaccuracies and provides that for $q = 0$ the correlation function should be equal 2. The λ factor appears also in the three-dimensional parametrization and for fully chaotic source the value of this factor is 1.

The R_{inv} parameter contains value of the size of the source averaged over the three dimensions. In case there is a lack measured data, which would be used to analysis by three dimensional function, it is only way, how to obtain information. A problem with the lack of data was mainly in the beginning of the RHIC start up. As time went on, the amount of available data grew and currently it is common to use a multidimensional correlation functions which provide more detailed characterization of the emitting source.

In the three-dimensional and in the Bertsch-Pratt coordinate system there is a parametrization, which makes possible to ascribed physical extensions to the employed parameters. In this case the parametrization of the correlation function is expressed [31] by

$$C(\vec{q}, \vec{K}) = 1 + \lambda(\vec{K}) \exp\left(-\sum_{i,j=o,s,l} R_{ij}^2(\vec{K}) q_i q_j\right), \quad (3.29)$$

generally depending on the 6 parameters R_{ij} .

In case of a midrapidity measurements parameters $R_{ol}^2 = R_{sl}^2 = 0$ and when the orientation of the event plane is known the correlation function is expressed

by

$$C(\vec{q}, \vec{K}) = 1 + \lambda(\vec{K}) \exp \left(-R_o^2(\vec{K})q_o^2 - R_s^2(\vec{K})q_s^2 - R_l^2(\vec{K})q_l^2 - 2R_{os}^2(\vec{K})q_oq_s \right). \quad (3.30)$$

In the absence of the azimuthal symmetry, there is not a symmetry in the parametrization of the correlation function, which would eliminated some parameters. The value of measured parameters depends on angles Φ , from which the source is observed as can be see in the Fig.3.4. In this case and if the LCMS is used, the parametrization is given by the same term like in the previous case. However the parameters R_{ij} depend not only on \vec{K} , but it is also function of azimuthal angle Φ . The R_{os} parameters is azimuthally sensitive and gives us the information about the azimuthal direction of the emitted particles. The Fig. 3.5 show STAR results from the study of the shape obtain from analysis the pion distribution [35].

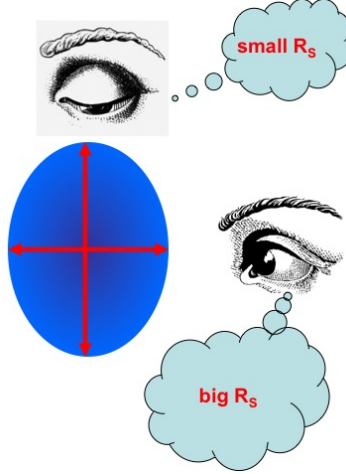


Fig. 3.4: Source size dependence on the angle Φ , from which the source is observed. Taken from [36].

In the absence of an information about event plane, the correlation function is averaged over all event plane orientation leading to $R_{os} = 0$ and the Eq. 3.29 is converted into the term

$$C(\vec{q}, \vec{K}) = 1 + \lambda(\vec{K}) \exp \left(-R_o^2(\vec{K})q_o^2 - R_s^2(\vec{K})q_s^2 - R_l^2(\vec{K})q_l^2 \right). \quad (3.31)$$

The significance of parameters is then following [37]:

$$\begin{aligned} R_o^2(\vec{K}) &= \langle (\tilde{x} - \beta_{\perp} \tilde{t})^2 \rangle \\ R_s^2(\vec{K}) &= \langle \tilde{y}^2 \rangle \\ R_l^2(\vec{K}) &= \langle (\tilde{z} - \beta_l \tilde{t})^2 \rangle \end{aligned} \quad (3.32)$$

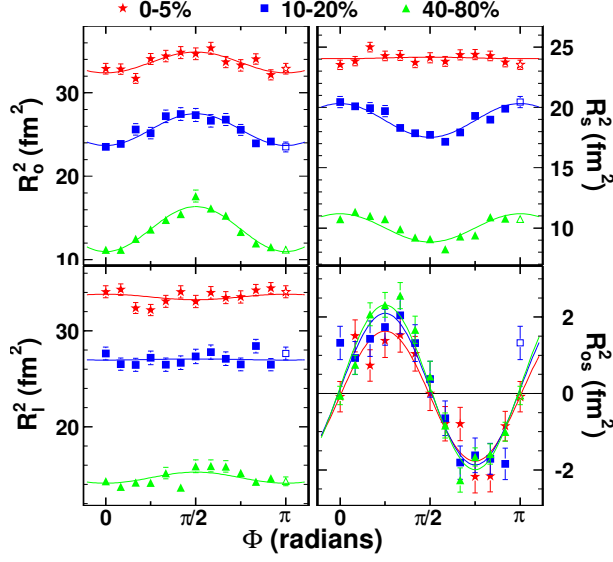


Fig. 3.5: The results of the measurement the HBT radii from the azimuthal sensitive analysis the pion distribution. Taken from [35]

where β_l is the longitudinal components of pair velocity and the β_\perp is the velocity of pair transverse to the beam (long) direction. The coordinates, which are noted by symbols \sim are the difference of the value of this coordinate and average value of this coordinate. According to this parametrization, it was shown [38], that difference

$$R_{diff} \equiv R_o^2 - R_s^2 = \beta_\perp^2 \langle \tilde{t}^2 \rangle - 2\beta_\perp \langle \tilde{x}\tilde{t} \rangle + \left(\langle \tilde{x}^2 \rangle - \langle \tilde{y}^2 \rangle \right), \quad (3.33)$$

where the first term is dominant and gives information about the lifetime of the source[39].

3.5 Femtoscopy measurements

In practice, when the correlation function is constructed from measured data, it is obtained as

$$C_{\vec{P}}^{ab}(\vec{q}) = \frac{A_{\vec{P}}^{ab}(\vec{q})}{B_{\vec{P}}^{ab}(\vec{q})} \xi_{\vec{P}}^{ab}(\vec{q}) = \frac{real\ pair}{mixed\ pair}, \quad (3.34)$$

where $A_{\vec{P}}^{ab}(\vec{q})$ is the signal distribution and refers to the relative momentum distribution of two particles, $B_{\vec{P}}^{ab}(\vec{q})$ is the uncorrelated background distribution and $\xi_{\vec{P}}^{ab}$ is a correction factor. The meaning of this equation is consistent with Eq.3.15, but there is the correction factor, which has the similar role as

the λ factor during the fitting. Symbols a , b , \vec{P} and \vec{q} mean that this correlation function deals with two particles a and b with pair momentum \vec{P} and relative momentum \vec{q} .

3.5.1 Signal Construction

The procedure of constructing the signal and background takes the following steps [32]:

1. Event quality cuts and event-class binning;
2. Single-track (including particle identification) cuts and single-particle binning
3. Two-particle pairing, two-track cuts and pair momentum binning.

In the first step, appropriate events fulfilling our request are chosen. These criteria can be for example the collision centrality, the reaction plane orientation and the vertex position. The events are usually divided into categories (bins) based on these selection criteria. Mixing together data from events which have different centrality or the vertex position could cause additional correlations which would make it hard or impossible to characterize their physical significance. It is important that this selection criteria also include conditions of detectors. These selected events are then used to construct the signal and background. For signal construction, which is then used for most femtoscopy analysis, the two-track acceptance is very important and has a very large effect on the correlation function. During the signal construction, there are two main complications, which could distort our data and for this reasons their effects have to be minimized.

One of them is split-tracks and merged-tracks. The split-track is a single track which is incorrectly reconstructed as a pair of tracks with low relative momenta. This can happen when particle is passing through the membrane in the TPC. Although it is only one track, detector can measure it as two tracks. One track ends close to the membrane on the one side of the membrane and second track starts in the same place, but behind the membrane.

On the other hand, there is also opposite problem - two tracks with similar trajectories can be reconstructed as a single track. This phenomenon leads to a loss of pairs with low relative momenta which in turn leads to an artificial decrease of the measured correlation function.

As it was previously mentioned, these effects have to be removed, thus there are pairwise cuts that remove these split-tracks and merge-tracks, which remained after the event-reconstruction algorithms. The more detailed description of the technique of removal split and merged tracks can be found in [40].

3.5.2 Background Construction

The background in Eq.3.34 has the same meaning as the denominator in Eq.3.15. One of the simplest way how to construct background is the event-mixing tech-

nique. For use this technique, there is one condition and it is that the effects energy-momentum conservation are negligible. This requirement can be satisfied in the high multiplicity environment. In case of low-multiplicity events or for elementary-particle collisions, by using event mixing the energy-momentum conservation can be violated and the correlation function obtained by the event-mixing technique would reflect non-femtoscopic correlations.

In the event-mixing technique the background pair distribution is created from the so called parent events. The single tracks from these parent events are mixed with other tracks from another parent event to create the uncorrelated distribution of pairs. The choice of the parent events is very important and not every event can be selected as the parent event. These events have to have the similar vertex positions, centrality, orientation the reaction plane ensuring, that the parents events have the same single-particle momentum distribution. When doing event mixing, there is also a requirement, that the parent events should have been measured close in time in order to have the same detector efficiencies. As can be seen, the selection of the parent events and the background construction is complicated, so there is also another way, how to obtain the background. One of possibility is that the background is constructed by pairs which are generated by Monte Carlo simulation. Also there exists another method called swapping by which the background can be constructed, but it is not widely used.

3.5.3 Corrections

Besides the signal and the background construction in Eq.3.34, there are corrections that have to be applied. These corrections can be divided into the 3 groups [32]:

1. finite resolutions effects;
2. misidentified particle contamination;
3. compensation for deficiencies in the background.

The first two corrections are caused by the fact, that our measurement will not be absolutely precise. By using modern technology these inaccuracies are reduced, but measurement with infinite accuracy will never be possible.

In the first case of these corrections, there is the problem with resolution with which the single-track momentum and the reaction plane can be measured. The resolution of the momentum measurement is the order of 1%. One of the possible way, how to reduce effect of this finite resolution is by using Monte Carlo simulation. In Monte Carlo simulation the correlation function with perfect momentum resolution and the correlation function, when the resolution momentum is finite can be generated. Then the double ratio of these functions can be calculated and used as a weight for this correction. Typically, the change in the final parameters obtained induced by this correction is smaller than 5%. In case of the azimuthally sensitive measurements the resolution of

the extracted event plane plays a role. The badly measured the reaction plane can affect the oscillations of the correlations functions, which leads to distortion of results.

There are other effects such as misidentified particles and non-primary particles, which come from decay of heavier particle which can impact the correlation function. The reason for this is that these particles are uncorrelated with other particles and decrease the magnitude of the correlation. Their effect can be eliminated by following procedure[40]

$$C^{true}(\vec{q}) = 1 + \frac{C^{raw}(\vec{q}) - 1}{\rho(\vec{q})}, \quad (3.35)$$

where C^{raw} is the correlation function, which is constructed without the correction and the purity ρ can be defined as

$$\rho = \frac{\text{correctly identified particle}}{\text{all detected particles}}. \quad (3.36)$$

On the other hand, the problem with misidentified particles can be removed by better detectors with better resolution. This solution can be demonstrated in the case of the STAR detectors, where the TOF detector was installed for the purpose of eliminating contamination by electron in the measured data, which can be use to the study of the K^+K^- correlations.

The effect of these deficiencies and application of the corrections can be seen in the Fig.3.6. Here is shown the correlation function prior and after the correction of purity and the correction of the momentum resolution was applied.

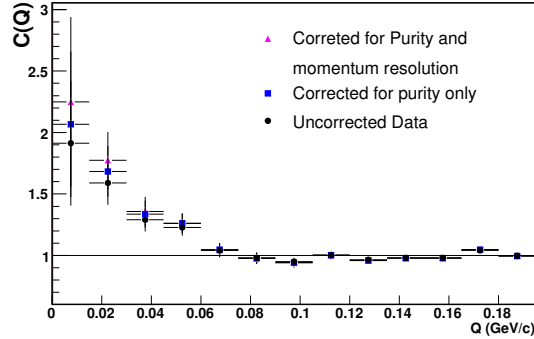


Fig. 3.6: The application of corrections on measured correlation function. Taken from [41] .

3.5.4 Fitting

Now, when the signal, the background and the corrections are prepared, the correlation function, which is given by Eq. 3.34, can be constructed. Then this

function will be used for fitting, by which the hidden information about the source parameters is obtained.

The simplest case is fitting by Eq.3.30 and Eq.3.31. To use these equations for fitting necessary assumptions are needed: that the source can be parametrized by Gaussian and the interaction between particles is described only by the quantum statistics. Thus the disadvantage of this fitting is the fact, that the Coulomb and strong interaction is neglected and this fit is limited for correlations of identical particles. Despite these disadvantages, this fit is very often used, because the fitting by Gaussian is very simple and can be done very fast by computer. For more precise results from the fitting, the Coulomb and strong interaction can not be neglected.

One of possible ways, which is referred as a standard procedure [31] and which do in a sense neglected the Coulomb interaction is fitting a Coulomb corrected correlation function [31] given by

$$C'(\vec{q}) = \frac{A(\vec{q})}{B(\vec{q})K_{coul}(q_{inv})} = 1 + \lambda \exp(-R_o^2 q_o^2 - R_s^2 q_s^2 - R_l^2 q_l^2), \quad (3.37)$$

where the $K_{coul}(q_{inv})$ is the squared Coulomb wave function, which is integrated over the whole source. As can be seen from the prescription of this equations, the Coulomb interactions is corrected in the denominator - the background, thus there have to be assumptions that all pairs in the background are primary pairs and have to be corrected.

Other possibility, how to perform the fitting is fitting by[31]

$$C(\vec{q}) = K'_{coul}(q_{inv}) \times (1 + \exp(-R_o^2 q_o^2 - R_s^2 q_s^2 - R_l^2 q_l^2)). \quad (3.38)$$

The Coulomb interaction and its correction is described by term

$$K'_{coul}(q_{inv}) = 1 + f(K_{coul}(q_{inv}) - 1), \quad (3.39)$$

where the influence of the Coulomb interaction is characterized by the parameter f . When there is not the Coulomb interaction, the value of parameter f is 0. On the other hand, the maximum value of f is 1 and corresponds to the standard weight of the Coulomb interaction. This procedure is called as dilution procedure [31].

Another, most often used, which can take into the account the effect of the Coulomb interaction is the Bowler-Sinyukov procedure. The name of this procedure refers to Bowler[42] and Sinyukov[43], whose observations are based of this procedure. The correlation function is fitted by

$$C(\vec{q}) = (1 - \lambda) + \lambda K_{coul}(q_{inv}) \times (1 + \exp(-R_o^2 q_o^2 - R_s^2 q_s^2 - R_l^2 q_l^2)). \quad (3.40)$$

This procedure was applied in analyzes, which are presented in [31] and [40], where can be found more detailed information about it. In the Fig 3.7 can be seen the comparison of the results from the fitting by the this procedure. As it was noted, each procedure needs some assumptions, which have to be satisfied.

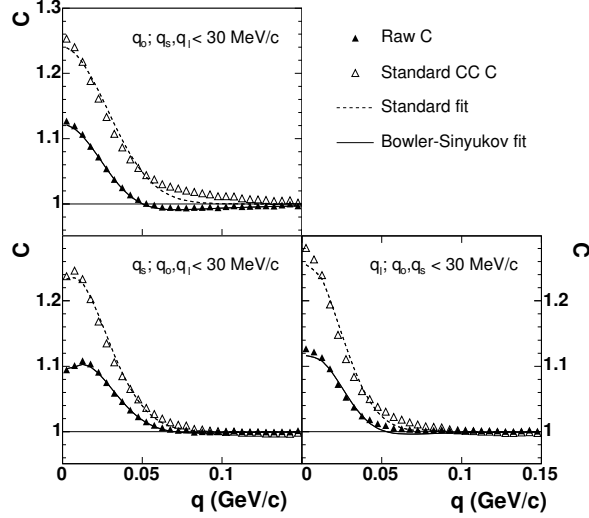


Fig. 3.7: The comparison of the results from the fitting. Taken from [40].

These assumptions affect results, but it is compensated by the fact, that using these procedures is not so time-consuming and computationally challenging.

The previous method was based on the fact that the analytic form of the function for the fitting was known. Sometimes however we do not have the knowledge and then another method has to be applied. This method is the numerical fitting. One of the program that is used in the correlation femtoscopy for numerical fitting is the CorrFit [44]. This program was developed by in C++ by Fabrice Retiere and expanded by Adam Kisiel. The CorrFit allows fitting without the knowledge of exact analytic form of the correlation function and uses only data available from the experiments. Unfortunately these facts make this approach quite time-consuming and CPU-intensive. Detailed description of this program can be found in [44] and results obtained from the fitting by the CorrFit can be found in [45].

Chapter 4

Effect of dynamics on measured HBT observables

4.1 First order phase transition and "HBT puzzle"

Up to the present time, the order of the phase transition from the confined hadronic gas to the QGP is not known and it is one of the questions of the current heavy ion physics. The first theoretical prediction, which was based on the hydrodynamic model, assumed the first order phase transition. The first order phase transition is for us well known as the transition from the ice to the water, when the latent heat is released.

It was predicted and shown [46], that the system, which undergoes first order phase transition has prolonged emission duration due to increasing entropy and it would influence the ratio R_o/R_s , which as show by the Eq.3.33 is sensitive to the emission duration. The value of this ratio should increase and be bigger than 1. This theoretical prediction is shown in the Fig. 4.1, where the R_o/R_s is function of the energy density in unit of Ts , where s is the entropy density.

The measurements during two decades, when the energy changed by two orders of magnitude, which are shown in the Fig. 4.2, do not show the predicted rapid increased of the ratio of R_o/R_s . This observation of no change in behaviour of R_o/R_s , which was in contrast with expectation is called as "HBT puzzle". Even sudden change of behaviour of any other parameter is not observed. The only observed change is a slight change in behaviour of parameters R_s and R_l which is expected to be related to a composition of the system which at low energy is dominated by protons and at high energy by pions. No observation of increase of the R_o/R_s ratio is understood as an evidence of nonexistence of the first order phase transition.

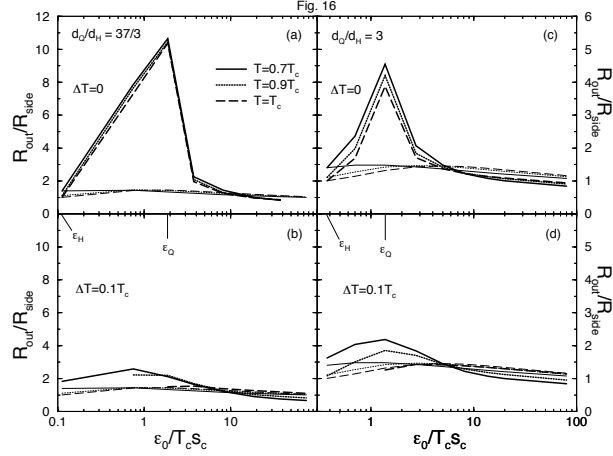


Fig. 4.1: Prediction of the first order phase transition. Taken from [46].

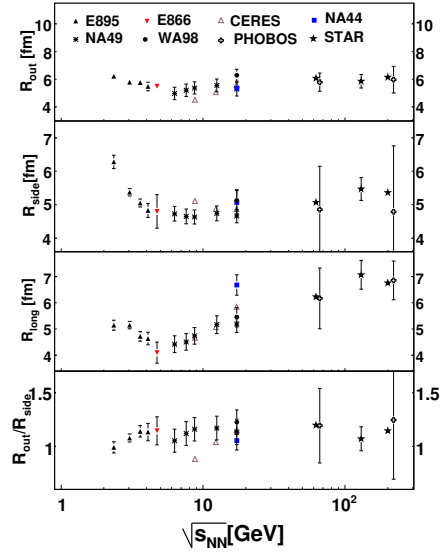


Fig. 4.2: Results from two last decades. Taken from [47].

4.2 Blast wave model/parametrization

It was shown how to extract from the measured data by fitting values of the parameters R_o^2 , R_s^2 and R_l^2 . To ascribe physical significance to these parameters it is suitable to remind the prescription of the correlation function, which was obtained by derivation described at the beginning of the previous chapter.

The correlation function is defined by Eq.3.19 for non-interaction particles when only the quantum statistics is used to construct the wave function. As it was mentioned the correlation function always depends on the relative source function denoted as $S_{\vec{K}}(\vec{r})$. Only this function is sensitive to the source size and only this function can give us the information about the space structure of the source. The relative source function depends on the relative distances of two emitted particles. During the derivation of the correlation function, *"the smoothness approximation"* was done. Thus the correlation of two particles, which are emitted close to each other and their momentum is approximately the same is studied.

The region, from which this pair of particles can be emitted is called *"the homogeneity region"* and its size is referred as *"the homogeneity length"*. Hence the measured values of the parameters R_o^2 , R_s^2 and R_l^2 contain the information about the size of this *"homogeneity region"*. It was also noted that the time-structure of the source is convoluted into the relative distance distribution function. From this follows that the full information about the space and time structure of the whole source can be obtained only by comparison of the measured parameters with models.

Although the evolution of the system can be described by hydrodynamics, the calculations with these models is complicated and the time-consuming. There are many models based on hydrodynamic equations that are used to characterize the source. These models necessarily employ simplification and the choice of the model depends on the situation which would be studied. For example the hydrodynamic transport models describe well the transverse mass spectra and elliptic flow, but their ability to describe pion source radii is not so good. Moreover their application for fitting of the correlation function is practically impossible.

For simple description and fitting of the correlation functions it is common to use a family of simplified models which use hydro-inspired parametrization of the particle emitting source.

There are many such models. Some of them can be quite sophisticated, including such effects like resonance and particle decay. Example of this model can be a HYDJET++[48]. In this thesis the blast wave model [49] of Retiere and Lisa which is the most commonly used one will be described in detail.

The blast wave model (the blast wave parametrization) describes the system at the time of thermal freeze-out. The parametrization contains 8 independent parameters, which are T , ρ_0 , ρ_2 , R_y , R_x , a_s , τ_0 and $\Delta\tau$. Their meaning is following [49]:

The transverse shape of the freeze-out distribution of the emission source, which has a temperature T , is described in the $(x - y)$ plane parameters R_x

and R_y . The emission source can be divided into the source elements and their spatial weighting is given by

$$\Omega(r, \phi_s) = \Omega(\tilde{r}) = \frac{1}{1 + e^{(\tilde{r}-1)/a_s}}, \quad (4.1)$$

where the normalized elliptical radius is defined as

$$\tilde{r}(r, \phi_s) \equiv \sqrt{\frac{(r \cos(\phi_s))^2}{R_x^2} + \frac{(r \sin(\phi_s))^2}{R_y^2}}. \quad (4.2)$$

The emission source has a surface diffuseness and its density profile is parametrized by a_s . The value of $a_s = 0$ corresponds to the uniform density profile and the Gaussian shape of the density profile is characterized by $a_s = 0.3$. The parameters ρ_0 and ρ_2 are used for calculation of the momentum spectrum of the emitted particles. Momentum spectrum is obtained by the thermal kinetic motion, which is boosted by a transverse rapidity $\rho(x, y)$. In case of the central collisions, the transverse rapidity is equal to ρ_0 in the outward direction and all the source elements on the outer edge are boosted by this transverse rapidity. For non-central collisions the situation is more complicated, because it has include dependence on the azimuthal angle ϕ_s . This depends is described by the parameter ρ_2 which describes the strength of the second-order oscillation of the transverse rapidity. Rapidity distribution of source elements is then express as

$$\rho(r, \phi_s) = \tilde{r}(\rho_0 + \rho_2 \cos(2\phi_s)), \quad (4.3)$$

where ϕ_b is the azimuthal direction of the boost and ϕ_s is the spacial azimuthal angle. It assumed that time dependence of emission function can be parametrized by Gaussian as

$$\frac{dN}{d\tau} \sim \exp\left(-\frac{(\tau - \tau_0)^2}{2\Delta\tau^2}\right), \quad (4.4)$$

where the τ_0 is time, when the source is emitting the particles and the $\Delta\tau$ is the lifetime of the source.

The model of the particle source is shown in the Fig. 4.3, where can be seen the illustration of a transversely expanding source with elliptical shape. On the right-hand side it can be seen homogeneity regions of the source from which the particle are emitted for the given emission direction.

With this model one can calculate prediction of p_T spectra, elliptic flow and their behaviour for different values of parameters. Most importantly the dependence of the HBT radii for different configurations can be studied in detail. The model allows to connect the HBT radii with their physical interpretation. For our purpose following results should be mentioned. It was shown, that the R_l^2 and R_o^2 are sensitive to timescale while R_s^2 contains only spacial information. From the model follows that the parameters R_l^2 can be expressed as

$$R_l^2(m_T) = \tau_0^2 \frac{T}{m_T} \times \frac{K_2(m_T/T)}{K_1(m_T/T)}, \quad (4.5)$$

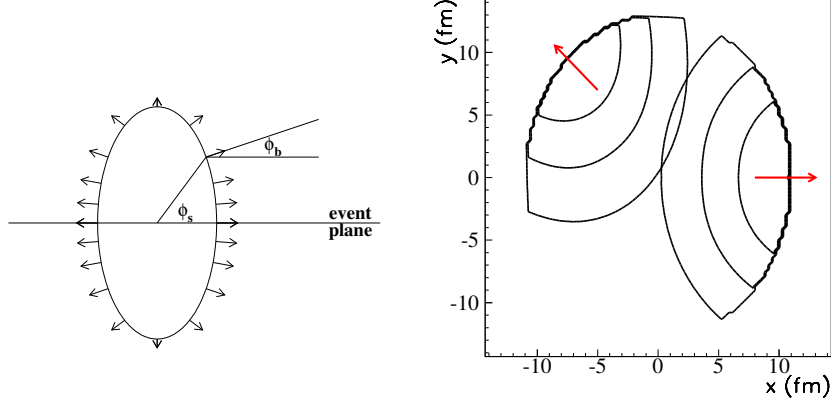


Fig. 4.3: The right-hand side: the illustration of an source. The left-hand side: the source, which was reconstructed by using two homogeneity regions, which was by measured particles, which were emitted at $\phi_p = 0^\circ$ and $\phi_p = 135^\circ$. Taken from [49].

where K_n are the modified Bessel functions. Thus for the fixed temperature T the lifetime of the source τ_0 can be obtained by the fitting the R_l^2 as a function of the m_T .

Another important effect is the so called "thermal smearing effect". It describes the influence of thermal motion on the observed size of the homogeneity region. The thermal smearing effect is caused by superposition of thermal motion, described by temperature T , with radial motion describe by parameter ϕ . Without the thermal motion all particles with the same momentum vector would be emitted from the same spatial point. However the thermal motion smears the point-like emission, creating a larger homogeneity region. The strength of this effect depends on particle mass and its velocity. The lighter particles in comparison with the heavier ones are smeared more over the volume of the source.

In general the measured size of the homogeneity region decreases with particle m_T . The mean emission point is shifted from the centre and the magnitude of the shift increases with m_T . Thus if the correlation between the lighter and slower particles is measured, the obtained value of parameters R_s^2 is larger. For low m_T on the order of energy of the thermal motion the homogeneity region is close to the size of the source. The thermal smearing effect and its dependence on the particle mass and velocity is illustrated in the Fig 4.4.

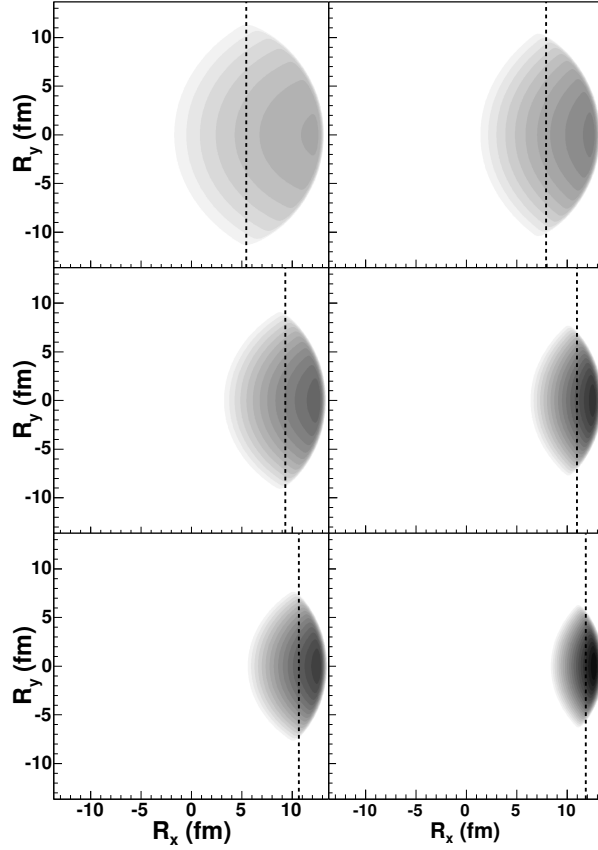


Fig. 4.4: The homogeneity region - the top panel is pion, the middle panel is for kaons and bottom for proton. Left-hand side is for $\beta_x = 0.907$ and the right-hand side is for $\beta_x = 0.974$. Taken from [49].

4.3 Collective behaviour - m_T scaling / m_T dependence

4.3.1 Longitudinal flow

The measured source undergoes space-time evolution and expands. The expansion of the source is characterized by the collective flow, which can be further divided by the direction of its action into the longitudinal and transverse flow. These two flows are the origin of the longitudinal x-p correlations and the transverse x-p correlation, respectively. Thus the information about the dynamic structure of the source are encoded into the HBT parameters, which are determined by these correlations.

The signature of the longitudinal flow is referred as " m_T scaling" [50], which is characterized by typical falling of the parameter R_l with p_T as $1/\sqrt{m_T}$.

The evidence of such a behaviour of R_l from different experiments is shown in Fig.4.5. This data set was made from the existing measurement of the pion radii by different experiments at the AGS, SPS and RHIC. For these measurement data were used from the most central Au+Au or Pb+Pb collisions. As can be seen from the Fig.4.5, for different energies, which change over two orders, the m_T dependence of R_l is surprisingly the same.

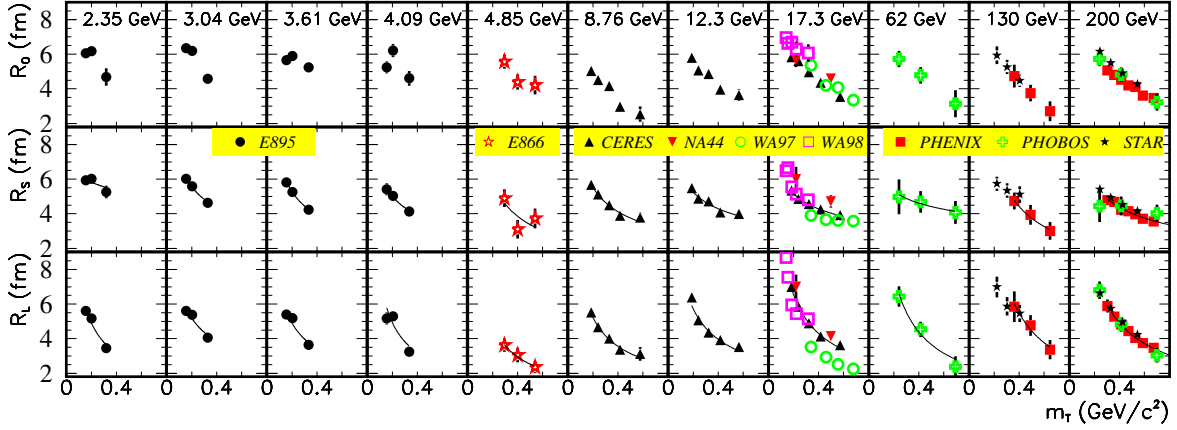


Fig. 4.5: World data set m_T dependence of HBT parameters. Taken from [32].

4.3.2 Transverse flow

The transverse flow[51] influences the parameters R_o and R_s . The strength of the transverse flow depends on the temperature of the expanding source and velocity of expansion. This dependence was discussed in the previous section, where it was noted as "*the thermal smearing effect*" and the conclusion, which claims that the parameters R_o and R_s decrease with m_T , was done. According to [52] the m_T dependence does not have to follow exactly $1/\sqrt{m_T}$ since it is a combination of dependence on temperature of the source and particle mass and its velocity.

In the Fig.4.5 can be seen the unambiguous m_T dependence of the radii. The universality of m_T dependence is shown in the Fig.4.6, where it is shown that the falling of the HBT radii, in this case R_{inv} , is the same for different particle species. The behaviour hold not only for particles with different mass, but also for particles that contain strange quarks. To indicate the universality of m_T dependence it was necessary to use the one-dimensional correlation function due to the fact, that the available statistic for correlation studies between less abundant particles, e.g. $p - \Lambda$, is limited.

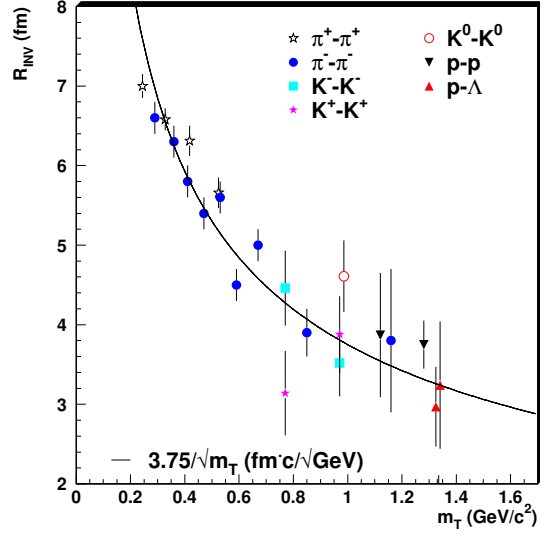


Fig. 4.6: The universality of m_T dependence for different particle mass. Taken from [52].

Another good test of transverse expansion of the system comes from non-identical particle correlations, by which we can study the predicted shift of the average emission point for different particle species. These measurements will be discussed in the next section.

Chapter 5

Non-identical particle correlations

5.1 Non-identical particle and correlation function

Up to now, the correlation function was constructed for two identical particles, but the correlation function can be deal with two non-identical particles as well. In comparison with identical particle correlation, by which the space-time structure of the source can be studied, the non-identical particle correlations provide a new information about the source - the emission asymmetries[53]. These asymmetries are result of dynamic evolution of the source. The asymmetries in emission can be of time and/or space character. Time asymmetries can be caused by the fact, that if two non-identical particles are emitted from the same point, the time of their emission can be different. This is especially interesting for multi-strange baryons, which can be emitted earlier than other baryons and hadrons. Their early emission is caused by their relative small cross section, thus they do not interaction with other particles, mainly with pions and can escape from the source. Spacial asymmetries are related with differential emission point of two non-identical particles at the same moment. One of the possible source of the spacial asymmetries is the effect of transverse flow. Another is a decay of long-lived resonance. These two asymmetries can be studied due to the fact, that two measured non-identical are identifiable.

In comparison with identical particle correlations, where the one correlation function is used, here it is necessary construct two correlation functions $C_+(\vec{k}^*)$ and $C_-(\vec{k}^*)$. As can be clear from using \vec{k}^* (see Eq.3.27), these correlations are studied in the pair rest frame. These two correlation functions describe two situations of correlation, which can occur. Let us have two non-identical particles and let us assume, that the first particle is emitted closer to the edge of the source and the emission point of the second is further to the edge of the

source. And now, two different situation can happen[54]. One of them, when the first particle has larger velocity than the second one, thus it will move away and the distance between them will become larger, the strength of interaction and correlation will diminish. Different situation can happen in case, that the first particle will be slower than the second particle. Due to its higher velocity, that the second particle will be catching up the first one up. At the moment of outrunning, their distance will be minimal and the correlation between them will be stronger and duration of interaction will be longer in comparison with the first case. These two situations are shown in the Fig.5.1.

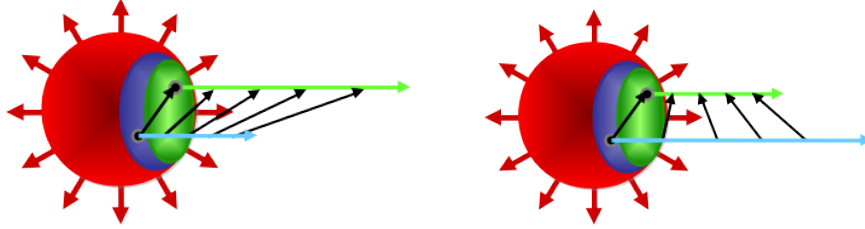


Fig. 5.1: The illustration of the emission and interaction of two non-identical particle. L: Faster particle is flying away and the interaction time is shorter. R:Faster particle is catching up and the interaction time is longer. Taken from [55] .

These two situations can be distinguished by out-component of \vec{k}^* . In first situation, $k_{out}^* > 0$ and it is described by the correlation function $C_-(\vec{k}^*)$, which is weaker than the correlation function $C_+(\vec{k}^*)$. This correlation function is for the second situation, when the one particle catch up the second one and this situation is characterized by $k_{out}^* < 0$. These two correlation functions are equal in case of that the average point of emission of two non-identical particle is the same [56].

To sum up, the measured pairs are divided into two groups according to the value of the k_{out}^* and relevant correlation function are constructed. Then the "double ratio" $C_+(\vec{k}^*)/C_-(\vec{k}^*)$ is constructed which is hence sensitive to the shift of mean emission point of each measured particle species. For reason of symmetries considerations and symmetric system with a symmetric rapidity [56]

$$\langle \Delta r_{side} \rangle = \langle \Delta r_{long} \rangle = 0. \quad (5.1)$$

Only asymmetries which can be observed are in out-direction:

$$\langle r_{out}^* \rangle = \langle \gamma (\langle \Delta r_{out} \rangle - \beta_{\perp} \langle \Delta t \rangle) \rangle, \quad (5.2)$$

where the superscript * denotes the distance of mean emission point in the pair rest frame. The fact of no expected asymmetries in side and long direction can

be used for testing of constructed correlation function, because the double ratio should equal one.

Example of non-identical particle correlations, which was studied, is pion-kaon correlations in central Au+Au collisions at $\sqrt{s_{NN}} = 130\text{GeV}$ [57] measured by the STAR experiment. Results of this analysis are shown in Fig.5.2, where both correlation functions can be seen - $C_+(k^*)$ and $C_-(k^*)$. In this Fig.5.2 can be also seen the correlation function denoted as $C(k^*)$, which is an average of the $C_+(k^*)$ and $C_-(k^*)$.

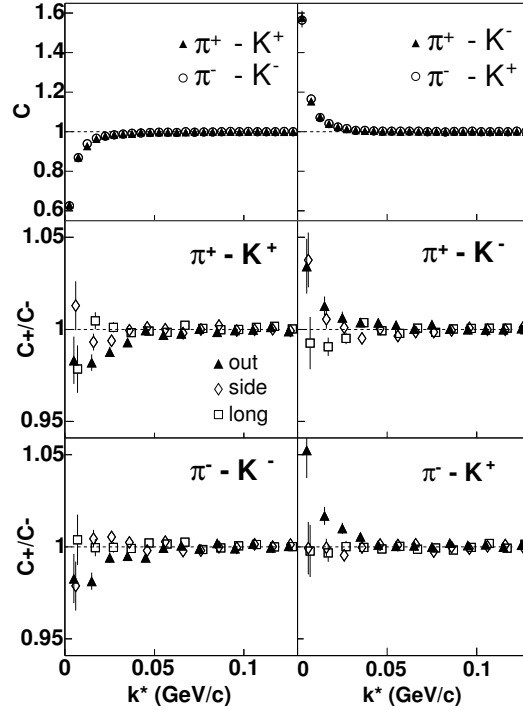


Fig. 5.2: Results of measured pion-kaon correlations. Top panel: correlation function $C(k^*)$, which is average of the $C_+(k^*)$ and $C_-(k^*)$. Middle and bottom panel: double ratio of correlation function $C_+(k^*)$ and $C_-(k^*)$. Taken from [57].

Fig.5.3 shows the comparison of results on the measured shifts of the mean emission point with model predictions. The model prediction was using the previously described blast wave parametrization and RQMD[58]. In addition to the blast wave, the RQMD provides not only the information about the shift of the mean emission point $\langle r_{out} \rangle$, abut also about the shift of the emission time $\langle \Delta t \rangle$. The results show the shift of the mean emission point for different particle species. As can be seen from the results, the magnitude of the shift larger for

particle species with higher difference of mass of particle. This is consistent with prediction, which was done by the blast wave model and are shown in the Fig.4.4, where the mean emission point for heavier particle is located closer to the edge of the source. These results can be understood as additional evidence of the transverse expansion of system that was created in the collisions of heavy ions.

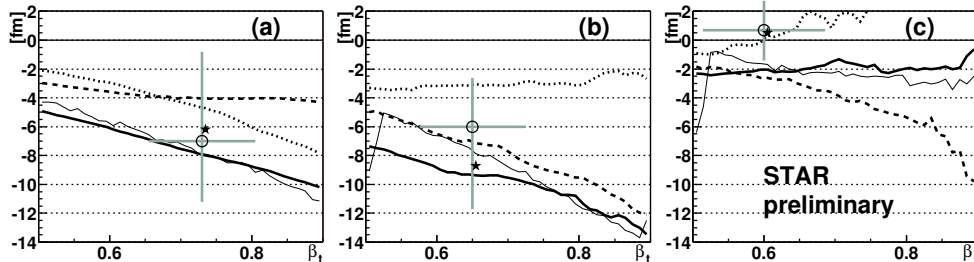


Fig. 5.3: Comparison of results ((a) pion-kaon, (b) pion-proton and (c) kaon-proton) of measured shifted mean emission point and time shifted with model prediction - blast wave parametrization (thin solid line) and RQMD(thick solid line). A space shifted in out direction (Δr_{out}) - dotted line. Time shifted (Δt) - dashed line. Taken from [56].

5.2 Results from rare and non-identical particle correlations measurements

Due to the high luminosity, which was achieved at the RHIC and LHC, it was possible to measure correlations between non-identical particles including the not so abundantly produced particle species. The overview of non-identical particle correlation measurements is shown in Table 5.1 which contains various particle combinations that were measured. Besides the non-identical particle measurement, there are also shown identical particle correlation measurements, which lie on the diagonal line.

The most traditional identical particle correlation measurements lie on the lowest part of the diagonal line. From them we can mention STAR results from $\pi - \pi$ correlations from Au+Au collisions at $\sqrt{s_{NN}} = 200\text{GeV}$ [59]. These measurements give general information about the source sizes. With the blast wave parametrization for azimuthally integrated pion HBT radii. It was measured that for the most central collision (centrality 0 – 5%) the radius of the source is $R = (13.3 \pm 0.2)\text{fm}$, the lifetime of the source $\tau = (9.0 \pm 0.3)\text{fm}/c$ and the emission duration $\Delta\tau = (2.83 \pm 0.19)\text{fm}/c$.

Additional interesting results can be obtained from non-identical measurements, which are sensitive not only to the size of the system, but also to an

	π^+	π^-	K^+	K^-	K_s^0	p	\bar{p}
Ξ^-	✓	✓					
Ξ^0	✓	✓					
Λ						✓	✓
Λ						✓	✓
\bar{p}	✓	✓	✓	✓		✓	✓
p	✓	✓	✓	✓		✓	
K_s^0					✓		
K^-	✓	✓		✓			
K^+	✓	✓	✓				
π^+	✓	✓					
π^-	✓						

Table 5.1: The overview of the femtoscopic studies. Taken from [52].

emission asymmetry between different particle species. In addition they can be used for studying the final state interaction(FSI), that is the strong interaction and Coulomb interaction for charged particles. From the listed non-identical correlation measurement, only the $\pi - \Xi$, $p - \Lambda$ and $K^0 - K^0$ correlations will be discussed in detail, because they can be used as good example of possibilities, what non-identical particle correlation measurements can provide.

5.2.1 $\pi - \Xi$ correlations

The STAR measurements on $\pi - \Xi$ correlations[34] [60] [61] were the first femtoscopic measurement with multi-strange baryons. The motivation for it is a testing of transverse expansion, and study of production of multi-strange baryons in heavy ion collisions and the FSI effects. As the multi-strange baryon, the Ξ^\pm was chosen. The second lighter non-identical particle was selected the π^\pm with mass $m = (139.57018 \pm 0.00035)\text{MeV}$ [2]. Since there is a large different in the mass of the particles the shift in the average emission point caused by transverse flow should be also large.

Authors of this analysis used a new technique[62] for the correlation function. This new technique is based on the fact that the angular part of the correlation function is decomposed into the 3D spherical harmonics, which are the function of angles φ and θ . By rewriting the components of \vec{k}^* into the spherical coordinate, which are described by two angles φ , θ and $|\vec{k}^*| = k^*$, the correlation function in the spherical coordinate system can be obtained. The advantage of this expression is the fact, that the correlation function [62]

$$C(k^*, \theta, \varphi) = \sqrt{4\pi} \sum_{l=0}^{\infty} \sum_{m=-l}^l A_{l,m}(k^*) Y_{l,m}^*(\theta, \varphi), \quad (5.3)$$

is a linear combination of the spherical harmonics $Y_{l,m}^*(\theta, \varphi)$. And the co-

efficients $A_{l,m}(k^*)$, which are function only one variable $|\vec{k}^*| = k^*$, contains the information about the source [63]. Spherical function $A_{l,m}$ have different symmetries and hence carry specific informations about the symmetries of the source. The monopole - $A_{0,0}$ - describes the size of the source while the dipole - $A_{1,1}$ - is sensitive to the shift of the mean emission points in out direction. The shape of the source is controlled by the values of the quadrupole - $A_{2,m}$. In comparison with the correlation function in variables from LCMS, this is more suitable, because it is reducing the problem with displaying three-dimensional correlation function into only a few one-dimensional plots.

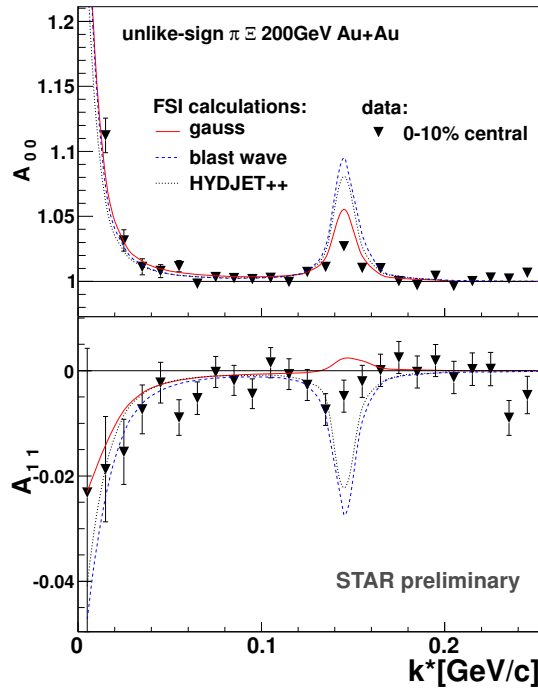


Fig. 5.4: Results and comparison of the 10% most central collision with theoretical calculations. Taken from [60] .

In case of no shift of the mean emission point the $A_{1,1}=0$. However as can be seen from the Fig.5.4, there is a significant shift of average point of emission. For 10% most central Au+Au collision was actually fitted as $\Delta r_{out} = (-5.6 \pm 1.0)$ fm. Negative value of the shifting shows, that mean emission point of the second particle, in this case Ξ , is closer to the edge of the source and the source of Ξ is smaller - $R = 2$ fm. By this measurement the radius of source in out direction was determined as $R_{out} = 10.2$ fm. Comparing these two values, it is clear, that the shift in emission is really extreme. This results agrees with our expectation, which could be gained from the Blastwave model shown in the Fig.4.4, where

the average point of emission of lighter particle is less shift than for the heavier particle.

For the case of $\pi - \Xi$ system these emission asymmetries, as authors noted and studied, can be also affected by the different decoupling conditions of different particle species. By using the HYDJET++[48], the authors studied and tested different freeze-out scenarios - single freeze-out, thermal freeze-out and early freeze-out scenario. The best results were achieved by the early freeze-out scenario, which were calculated with the assumption, that the Ξ and $\Xi^*(1530)$ resonance are emitted at chemical freeze-out at $T_{ch} = 165\text{MeV}$ and the other particle species are emitted at the thermal freeze-out, which occurs at $T_{th} = 100\text{MeV}$. This difference in the emission times is then also part of the observed shift.

The $\pi - \Xi$ correlation function contains also one more interesting part. As can be seen from in Fig.5.4 the theoretical calculations describe well low k^* region of the correlation function which is dominated by the Coulombomb interaction. However they fail to describe higher $k^* \sim 150\text{ MeV}$ which is dominated $\Xi^*(1530)$ resonance. The resonance $\Xi^*(1530)$ is a result of the strong FSI between π and Ξ . This shows that we so far do not fully understand how to treat the strong FSI interaction for resonances in the correlation function. Hence study of strong final state interaction between particles using the HBT formalism is open topic for research.

5.2.2 $K^0 - K^0$ correlations

The STAR measurements of $K_s^0 - K_s^0$ correlations[41] were used not to only obtain the source size, but also to study the effects of the strong FSI.

The source size is usually obtained from the $\pi - \pi$ measurement, because pions are produced in a huge multiplicities in nucleus-nucleus collisions. These measurement are however complicated due to the fact, that many pions can come from the decays of resonances. As the result of this there can be a problem with fitting by Gaussian function. Moreover the pions can be identify via dE/dx only up to $700\text{MeV}/c$. Compared with it the neutral kaons are reconstructed by their decay topology which allows to identify the neutral kaons at higher momentum. In addition the kaons they are less affected by the decay of resonances.

Using the neutral kaons with the mean transverse mass $\langle m_T \rangle = 1.07\text{GeV}$ the radius of the source was measured as $R = 4.09 \pm 0.46(stat) \pm 0.31(sys)\text{fm}$. This result is qualitatively consistent with the established m_T -dependence from the $\pi - \pi$ measurements. It is hence another crosscheck of the observed transverse expansion of the source.

In addition, as was already mentioned, the $K^0 - K^0$ correlation was used for studying strong FSI. The neutral kaons can be further divided into two group - short lived neutral kaons K_s^0 and long lived neutral kaons K_l^0 . Both of them are the combination of the kaon and antikaon. The state vector of the short

and long lived neutral kaons are

$$\begin{aligned} |K_s^0\rangle &= \frac{1}{\sqrt{2}} (|K^0\rangle + |\bar{K}^0\rangle), \\ |K_l^0\rangle &= \frac{1}{\sqrt{2}} (|K^0\rangle - |\bar{K}^0\rangle), \end{aligned} \quad (5.4)$$

where the $|K^0\rangle$, $|\bar{K}^0\rangle$ are the state vector of the kaon and antikaon respectively. Thus the state vector of the $K_s^0 K_s^0$ is

$$|K_s^0 K_s^0\rangle = \frac{1}{2} (|K^0 K^0\rangle + |K^0 \bar{K}^0\rangle + |\bar{K}^0 K^0\rangle + |\bar{K}^0 \bar{K}^0\rangle). \quad (5.5)$$

The $K_s^0 K_s^0$ can come from the $K^0 K^0$ pair, $\bar{K}^0 \bar{K}^0$ pair or the pair of two non-identical particle $K^0 \bar{K}^0$. It was shown in [64], that the contribution of the $K^0 \bar{K}^0$, which influences the $K_s^0 K_s^0$, come only from the symmetric part of the $K^0 \bar{K}^0$ amplitude. Also these pairs are affected by the resonances $f_0(980)$ and $a_0(980)$. The results of this effect is the domination of the imaginary part of $\sim 1\text{fm}$ in the s-wave scattering length.

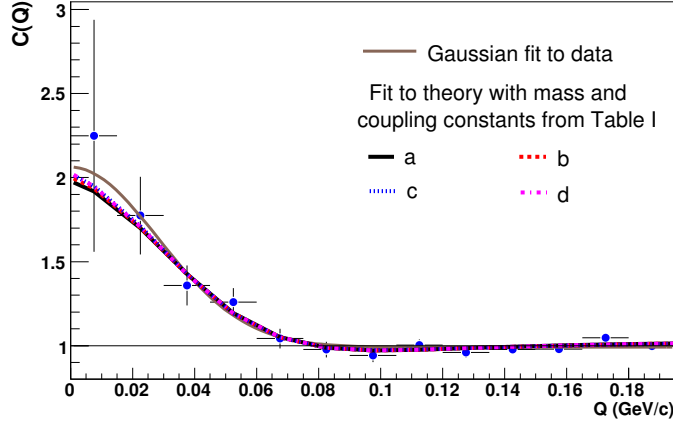


Fig. 5.5: Fitting by Gauss and the correlation functions, which take into account the FSI. Taken from [41].

Hence the $K_s^0 - K_s^0$ correlations can be used to study the effects of these two resonances on extracted size of the source.

The obtained correlation function was studied for different values of parameters characterizing both of the resonances (masses, couplings). As can be seen in the Fig 5.5, different set of values of these parameters were used and to calculate and fit the theoretical shape of the correlation functions to the measured data. The radius of the source, which is obtained by fitting the correlation

function, which include effect of resonances, is smaller in comparison with the results from simple the Gaussian fit of the non-interacting particles. This analysis demonstrates how the femtoscopy can be used to study the strong final state interaction.

5.2.3 $p - \Lambda$ correlations

As in the previous measurement, the main goal of the STAR $p - \Lambda$ analysis[65] was to study the effect of FSI. But in this case it was the baryon-antibaryon strong interaction. The motivation for this studies is the fact, that the results from $p - \bar{\Lambda}$ and $\bar{p} - \Lambda$ correlation function, which were obtained for the first time and showed the large anti-correlation, were not consistent with the results from $p - \Lambda$ and $\bar{p} - \bar{\Lambda}$ correlation function. It was clear that this inaccuracy comes from the unknown strong interaction potential for $p - \bar{\Lambda}$ and $\bar{p} - \Lambda$ respectively and unknown baryon-antibaryon annihilation cross section. In the past the only studied strong interaction potential between baryon and antibaryon was in $p - \bar{p}$ system.

The experimental approach was similar as in the $K_s^0 - K_s^0$ analysis. Due to the fact, that the interaction potentials for $p - \Lambda$ and $\bar{p} - \bar{\Lambda}$ is known the scattering length f_0 was not the free parameters during fitting and the radius r_0 of the source was obtained from the fit without a problem.

Because $\bar{p} - \Lambda$ and $p - \bar{\Lambda}$ scattering lengths f_0 are unknown and were never measured before were the free parameters in the fitting of the correlation function. The Fig.5.6 shows the comparison of the fitted scattering length f_0 with measurements for the $p - \bar{p}$. As can be seen, the imaginary part of scattering length f_0 , which describe the annihilation, agrees with the value measured in $p - \bar{p}$ systems, but the value of real part of f_0 is smaller.

Although the scattering length was determined, the value of radius r_0 of the source from the both of the $p - \bar{\Lambda}$ and $\bar{p} - \Lambda$ correlation function were inconsistent with the value from the $p - \Lambda$ and $\bar{p} - \bar{\Lambda}$ correlation function. Improving this analysis was presented in [66], where authors are using the correlation function which is corrected for residual correlation. These residual correlations arise from detecting daughter particles from decays of primary pairs which are correlated. Part of this correlation then carried on by the daughter particles from which we construct the final correlation function. By using the residual correlation, the new value of the real and imaginary part of the scattering length was obtained and the radius r_0 of the source which is in the agreements with the results from $p - \Lambda$ and $\bar{p} - \bar{\Lambda}$ correlation function was obtained.

We can see that that femtoscopy can serve not only as a way to measure the size and emission asymmetries of the source, but it can also be utilize to study otherwise hardly accessible interaction between different particle species.

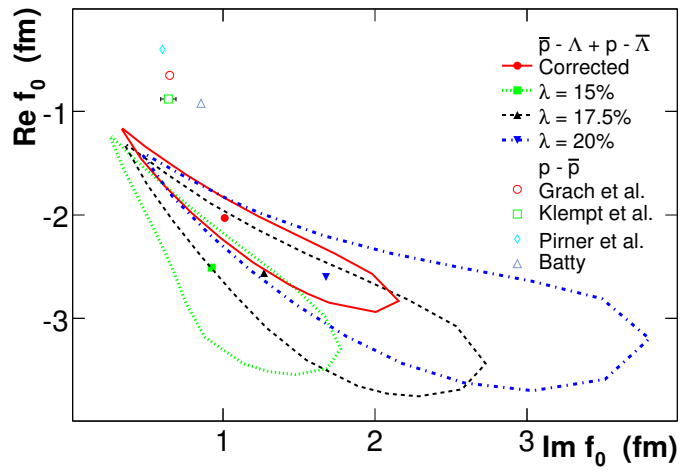


Fig. 5.6: Comparison measured scattering length with results from $p-\bar{p}$ system. By the curves, the one standard deviation contours is showed. Taken from [65]

Chapter 6

Conclusions

The main goal of this bachelor thesis was to introduce the correlation femtoscopy and its application in the study of the system which is formed during heavy ion collisions.

Quantum chromodynamics predicts that at high temperature and density a new state of the matter - quark-gluon plasma can be formed. This very hot and dense state of matter, as it is predicted, existed a few microseconds after the Big bang. On the Earth it can be studied in heavy ion collisions, which take place e.g. at the Relativistic heavy ion collider in Brookhaven Nationality Laboratory. In this thesis, description of the heavy ion collisions, the quark-gluon plasma and its signatures were discussed.

Relativistic Heavy Ion Collider(RHIC) at Brookhaven National Laboratory is a facility dedicated to the study of a matter created in ultra-relativistic collisions of heavy nuclei. STAR experiment is of the two main detectors at the RHIC. In this thesis the STAR detector with its main subdetectors is described. The discussion also includes recent and planned upgrades of the detector and RHIC.

Correlation femtoscopy allows to study the characteristic space-time extents of the created system by measuring correlations between particles with small relative momenta. The typical sizes of the particle-emitting source are on the order of unit up to tens of Fermi. In this thesis, the derivation of the two-particle correlation function is reviewed. The process of experimental construction of the two-particle correlation function is discussed in details together with all the necessary corrections that usually need to be performed. Also the parametrization of the correlation function and the fitting procedure which is used to extract the physics information is presented.

It is shown that the correlation function is sensitive only to a distribution of relative distances of the emission points. In order to obtain full information about the source size and its evolution a comparison to models has to be used. One of the most commonly used model is the so called "blast wave parametrization" which is used in this work to make a connection between measured radii and their physical interpretation.

Due to the high luminosity, which was achieved in the RHIC in the last ten years, it is newly possible to study correlations between the non-identical particles. The difference in the construction of the correlation function for non-identical and identical particle is discussed. In comparison with the identical particles the non-identical particle correlations allow besides the information about the source size also allow to extract information about the space-time emission asymmetries. Since these asymmetries are caused dynamic effects during the evolution of the system the femtoscopic measurements can be used to study dynamical properties of the system, such as transverse flow and freeze-out conditions. Also, as it is discussed, the non-identical particle correlations measurements provide the information about the final state interaction which is often hard to access in classical scattering experiments. Results of STAR experiment on non-identical correlations are hence presented and discussed.

Since it's first use in the 1960's the correlation femtoscopy has become an indispensable tool in the field of heavy-ion physics. Due to high luminosities of current colliders we can expect the femtoscopy to continue deliver important physics results also in the future.

Appendices

Appendix A

The RHIC Run Overview

Run	Year	Species	$\sqrt{s_{NN}}$ (GeV)	Delivered Luminosity
1	2000	Au+Au	56.0	$<0.001\mu\text{b}^{-1}$
		Au+Au	130.0	$20\mu\text{b}^{-1}$
2	2001/2002	Au+Au	200.0	$258\mu\text{b}^{-1}$
		Au+Au	19.6	$0.4\mu\text{b}^{-1}$
		p+p	200.4	1.4pb^{-1}
3	2003	d+Au	200.0	73nb^{-1}
		p+p	100.4	5.5pb^{-1}
4	2004	Au+Au	200.0	3.53nb^{-1}
		Au+Au	62.4	$67\mu\text{b}^{-1}$
		p+p	200.4	7.1pb^{-1}
5	2005	Cu+Cu	200.0	42.1nb^{-1}
		Cu+Cu	62.4	1.5nb^{-1}
		Cu+Cu	22.4	0.02nb^{-1}
		p+p	200.4	29.5pb^{-1}
		p+p	409.8	0.1pb^{-1}
6	2006	p+p	200.4	88.6pb^{-1}
		p+p	62.4	1.05pb^{-1}
7	2007	Au+Au	200.0	7.25nb^{-1}
		Au+Au	9.2	small
8	2008	d+Au	200.0	437nb^{-1}
		p+p	200.4	38.4pb^{-1}
		Au+Au	9.2	small
9	2009	p+p	499.8	110pb^{-1}
		p+p	200.4	114pb^{-1}
		pp2pp	200.4	0.6nb^{-1}

Table A.1: The RHIC Run Overview. Taken from [67].

Run	Year	Species	$\sqrt{s_{NN}}$ (GeV)	Delivered Luminosity
10	2010	Au+Au	200.0	10.3nb^{-1}
		Au+Au	62.4	$544\mu\text{b}^{-1}$
		Au+Au	39.0	$206\mu\text{b}^{-1}$
		Au+Au	3.7	$4.23\mu\text{b}^{-1}$
		Au+Au	11.0	$7.8\mu\text{b}^{-1}$
11	2010/2011	p+p	499.8	166pb^{-1}
		Au+Au	19.6	$33.2\mu\text{b}^{-1}$
		Au+Au	200.0	9.79nb^{-1}
		Au+Au	27.0	$63.1\mu\text{b}^{-1}$
12	2012	p+p	200.4	74.0pb^{-1}
		p+p	499.8	283pb^{-1}
		U+U	192.8	$736\mu\text{b}^{-1}$
		Cu+Au	200.0	27.0nb^{-1}
13	2013	p+p	499.8	1100pb^{-1}
14	2014	Au+Au	14.6	$44.2\mu\text{b}^{-1}$
		Au+Au	200.0	$45.1\mu\text{b}^{-1}$

Table A.2: The RHIC Run Overview. Taken from [67].

Bibliography

- [1] Ivan Štoll. *The history of physics*. Prometheus, 2009.
- [2] K. Nakamura et al. Review of particle physics. *J.Phys.*, G37:075021, 2010.
- [3] Wikimedia Commons. Standard model. http://upload.wikimedia.org/wikipedia/commons/0/00/Standard_Model_of_Elementary_Particles.svg, [Online 6-March-2014].
- [4] David J. Gross and Frank Wilczek. Ultraviolet behavior of non-abelian gauge theories. *Phys. Rev. Lett.*, 30:1343–1346, Jun 1973.
- [5] Nobel Media. The nobel prize in physics 2004 - advanced information. http://http://www.nobelprize.org/nobel_prizes/physics/laureates/2004/advanced.html, [Online 12-April-2014].
- [6] F. Karsch, E. Laermann, and A. Peikert. Quark mass and flavor dependence of the QCD phase transition. *Nucl.Phys.*, B605:579–599, 2001.
- [7] BNL. Rhic accelerators. <http://www.bnl.gov/rhic/complex.asp>, [Online 6-March-2014].
- [8] C.Y. Wong. *Introduction to high-energy heavy-ion collisions*. World Scientific Pub Co, 1990.
- [9] Reinhard Stock. Relativistic Nucleus-Nucleus Collisions and the QCD Matter Phase Diagram. 2008.
- [10] IOP science. The collision of two nuclei. <http://ej.iop.org/images/1367-2630/13/5/055008/Full/nj384456fig2.jpg>, [Online 13-March-2014].
- [11] Michael Kliemant, Raghunath Sahoo, Tim Schuster, and Reinhard Stock. Global Properties of Nucleus-Nucleus Collisions. *Lect. Notes Phys.*, 785:23–103, 2010.
- [12] Brookhaven National Laboratory. Laboratory, brookhaven national. <http://www.star.bnl.gov>, [Online 10-March-2014].

- [13] Michal Sumbera. Results from STAR Beam Energy Scan Program. *Acta Phys.Polon.Supp.*, 6:429–436, 2013.
- [14] Peter Jacobs and Xin-Nian Wang. Matter in extremis: Ultrarelativistic nuclear collisions at RHIC. *Prog.Part.Nucl.Phys.*, 54:443–534, 2005.
- [15] K. Adcox et al. PHENIX detector overview. *Nucl.Instrum.Meth.*, A499:469–479, 2003.
- [16] K.H. Ackermann et al. STAR detector overview. *Nucl.Instrum.Meth.*, A499:624–632, 2003.
- [17] M. Anderson, J. Berkovitz, W. Betts, R. Bossingham, F. Bieser, et al. The Star time projection chamber: A Unique tool for studying high multiplicity events at RHIC. *Nucl.Instrum.Meth.*, A499:659–678, 2003.
- [18] H. Bichsel. A method to improve tracking and particle identification in TPCs and silicon detectors. *Nucl.Instrum.Meth.*, A562:154–197, 2006.
- [19] L. Adamczyk et al. Elliptic flow of identified hadrons in Au+Au collisions at $\sqrt{s_{NN}} = 7.7\text{-}62.4$ GeV. *Phys.Rev.*, C88(1):014902, 2013.
- [20] W.J. Llope. The large-area time-of-flight upgrade for STAR. *Nucl.Instrum.Meth.*, B241:306–310, 2005.
- [21] Christopher Beresford Powell. *J/ψ Production in Heavy Ion Collisions at the STAR detector at RHIC*. PhD thesis, University of Cape Town, 2012.
- [22] M. Beddo et al. The STAR barrel electromagnetic calorimeter. *Nucl.Instrum.Meth.*, A499:725–739, 2003.
- [23] F.S. Bieser, H.J. Crawford, J. Engelage, G. Eppley, L.C. Greiner, et al. The STAR trigger. *Nucl.Instrum.Meth.*, A499:766–777, 2003.
- [24] J.M. Landgraf et al. An overview of the STAR DAQ system. *Nucl.Instrum.Meth.*, A499:762–765, 2003.
- [25] L. Ruan, G. Lin, Z. Xu, K. Asselta, H.F. Chen, et al. Perspectives of a Midrapidity Dimuon Program at RHIC: A Novel and Compact Muon Telescope Detector. *J.Phys.*, G36:095001, 2009.
- [26] Spiros Margetis. Heavy Flavor Tracker (HFT): The new silicon vertex detector for the STAR experiment at RHIC. *Nucl.Phys.Proc.Suppl.*, 210-211:227–230, 2011.
- [27] A. Shabetai. The hft, a heavy flavor tracker for star. *The European Physical Journal C*, 49(1):169–175, 2007.
- [28] A. Accardi, J.L. Albacete, M. Anselmino, N. Armesto, E.C. Aschenauer, et al. Electron Ion Collider: The Next QCD Frontier - Understanding the glue that binds us all. 2012.

- [29] Robert Hanbury; Richard Q. Twiss Brown. A test of new type of stellar interferometer on sirius. *Nature*, 178(4541):1046–1048, 1956.
- [30] Gerson Goldhaber". Influence of bose-einstein statistics on the antiproton-proton annihilation process. *Physical Review*, 120(1):300–312, 1960.
- [31] Mercedes Lopez Noriega. *Pion Interferometry in AuAu Collisions at a Center of Mass Energy per Nucleon of 200 GeV*. PhD thesis, The Ohio State University, 2004.
- [32] Michael Annan Lisa, Scott Pratt, Ron Soltz, and Urs Wiedemann. Femtoscopy in relativistic heavy ion collisions. *Ann.Rev.Nucl.Part.Sci.*, 55:357–402, 2005.
- [33] D. Anchishkin, Ulrich W. Heinz, and P. Renk. Final state interactions in two particle interferometry. *Phys.Rev.*, C57:1428–1439, 1998.
- [34] Petr Chaloupka. *Femtoscopy with multi-strange baryons at RHIC*. PhD thesis, Charles University in Prague, 2010.
- [35] J. Adams et al. Azimuthally sensitive HBT in Au + Au collisions at $s(NN)^{1/2} = 200$ -GeV. *Phys.Rev.Lett.*, 93:012301, 2004.
- [36] Michael Annan Lisa. Femtoscopy in relativistic heavy ion collisions. The Berkeley School - Femtoscopy, 2005.
- [37] Ulrich W. Heinz. How to extract physics from HBT radius parameters. *Nucl.Phys.*, A610:264C–277C, 1996.
- [38] T. Csorgo and S. Pratt. Structure of the peak in Bose-Einstein correlations. *Conf.Proc.*, C9106175:75–90, 1991.
- [39] Y.F. Wu, Ulrich W. Heinz, B. Tomasik, and U.A. Wiedemann. Yano-Koonin-Podgoretskii parametrization of the HBT correlator: A Numerical study. *Eur.Phys.J.*, C1:599–617, 1998.
- [40] J. Adams et al. Pion interferometry in Au+Au collisions at $S(NN)^{1/2} = 200$ -GeV. *Phys.Rev.*, C71:044906, 2005.
- [41] B.I. Abelev et al. Neutral kaon interferometry in Au+Au collisions at $s(NN)^{1/2} = 200$ -GeV. *Phys.Rev.*, C74:054902, 2006.
- [42] M.G. Bowler. Coulomb corrections to bose-einstein corrections have greatly exaggerated. *Physics Letters B*, 270(1):69 – 74, 1991.
- [43] Yu. Sinyukov, R. Lednicky, S.V. Akkelin, J. Pluta, and B. Erazmus. Coulomb corrections for interferometry analysis of expanding hadron systems. *Phys.Lett.*, B432:248–257, 1998.
- [44] Adam Kisiel, editor. *CorrFit: a program to fit arbitrary two-particle correlation functions*, volume 49(Supplement 2). Nukleonika, 2004.

- [45] Adam Kisiel. Non-identical particle femtoscopy in models with single freeze-out. *Braz.J.Phys.*, 37:917–924, 2007.
- [46] Dirk H. Rischke and Miklos Gyulassy. The Time delay signature of quark - gluon plasma formation in relativistic nuclear collisions. *Nucl.Phys.*, A608:479–512, 1996.
- [47] B.I. Abelev et al. Pion Interferometry in Au+Au and Cu+Cu Collisions at RHIC. *Phys.Rev.*, C80:024905, 2009.
- [48] I.P. Lokhtin, L.V. Malinina, S.V. Petrushanko, A.M. Snigirev, I. Arsene, et al. Heavy ion event generator HYDJET++ (HYDrodynamics plus JETs). *Comput.Phys.Commun.*, 180:779–799, 2009.
- [49] Fabrice Retiere and Michael Annan Lisa. Observable implications of geometrical and dynamical aspects of freeze out in heavy ion collisions. *Phys.Rev.*, C70:044907, 2004.
- [50] A.N. Makhlin and Yu.M. Sinyukov. Hydrodynamics of Hadron Matter Under Pion Interferometric Microscope. *Z.Phys.*, C39:69, 1988.
- [51] S. Pratt. Pion Interferometry for Exploding Sources. *Phys.Rev.Lett.*, 53:1219–1221, 1984.
- [52] Michael Annan Lisa and Scott Pratt. Femtoscopically Probing the Freeze-out Configuration in Heavy Ion Collisions. 2008.
- [53] R. Lednicky, V.L. Lyuboshits, B. Erazmus, and D. Nouais. How to measure which sort of particles was emitted earlier and which later. *Phys.Lett.*, B373:30–34, 1996.
- [54] Hanna Zbroszczyk. *Studies of Baryon-Baryon Correlations in Relativistic Nuclear Collisions Registered at the STAR Experiment*. PhD thesis, Warsaw University of Technology, 2008.
- [55] Petr Chaloupka. Measuring of emission source size by pi-xi correlation. Mala Skala 2011.
- [56] Adam Kisiel. Nonidentical particle correlations in 130-A-GeV and 200-A-GeV collisions at STAR. *J.Phys.*, G30:S1059–S1064, 2004.
- [57] J. Adams et al. Pion kaon correlations in Au+Au collisions at $\sqrt{s(NN)}^{*1/2} = 130$ -GeV. *Phys.Rev.Lett.*, 91:262302, 2003.
- [58] H. Sorge. Flavor production in Pb (160-A/GeV) on Pb collisions: Effect of color ropes and hadronic rescattering. *Phys.Rev.*, C52:3291–3314, 1995.
- [59] J. Adams et al. Pion interferometry in Au+Au collisions at $\sqrt{s(NN)}^{*(1/2)} = 200$ -GeV. *Phys.Rev.*, C71:044906, 2005.

- [60] Petr Chaloupka. Femtoscopy with multi-strange baryons at RHIC. *Phys.Part.Nucl.Lett.*, 8:973–976, 2011.
- [61] P. Chaloupka, M. Sumbera, and L.V. Malinina. pi Xi correlations: Model comparison and Xi*(1530) puzzle. *Acta Phys.Polon.*, B40:1185–1192, 2009.
- [62] Z. Chajeccki, T.D. Gutierrez, M.A. Lisa, and M. Lopez-Noriega. AA versus PP (and dA): A Puzzling scaling in NBT and RHIC. 2005.
- [63] D. A. Brown, A. Enokizono, M. Heffner, R. Soltz, P. Danielewicz, and S. Pratt. Imaging three dimensional two-particle correlations for heavy-ion reaction studies. *Phys. Rev. C*, 72:054902, Nov 2005.
- [64] Miklos Gyulassy. K(s) pictures of strangeness distillation. *Phys.Lett.*, B286:211–215, 1992.
- [65] J. Adams et al. Proton - lambda correlations in central Au+Au collisions at $S(NN)^{1/2} = 200$ -GeV. *Phys.Rev.*, C74:064906, 2006.
- [66] Adam Kisiel, Hanna Zbroszczyk, and Maciej Szymanski. Extracting baryon-antibaryon strong interaction potentials from p Λ femtoscopic correlation function. *Phys.Rev.*, C89:054916, 2014.
- [67] Wolfram Fischer. The rhic run overview. <http://www.agsrhichome.bnl.gov/RHIC/Runs/>, [Online 4-July-2014].